INSTITUTE

FOR

AEROSPACE STUDIES

UNIVERSITY OF TORONTO
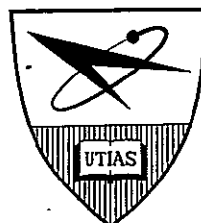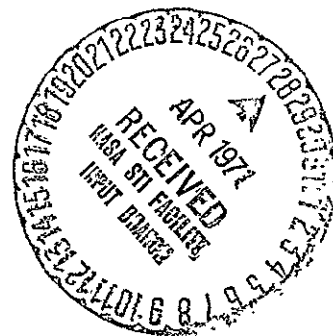
APPRAISAL OF UTIAS IMPLOSION-DRIVEN

HYPERVELOCITY LAUNCHERS AND SHOCK TUBES

by

I. I. Glass

UTIAS

June, 1970.

UTIAS Review No. 31

ACKNOWLEDGEMENTS

TABLE OF CONTENTS

ii.

SUMMARY

A critical appraisal is made of the design, research, development, and operation of the novel UTIAS Implosion-Driven Hypervelocity Launchers and Shock Tubes. Explosively-driven (PbN_6-lead azide, PETN-pentaerythritetetranitrate) implosions in detonating stoichiometric hydrogen-oxygen mixtures have been successfully developed as drivers for hypervelocity launchers and shock tubes in a safe and reusable facility. Intense loadings at very high calculated pressures (almost megabar range), densities (g/cm^3) and temperatures (thousands °K), at the implosion centre, cause severe problems with projectile integrity. Misalignment of the focal point can occur and add to the difficulty in using small calibre (6 to 8 mm dia) projectiles. In addition, the extreme driving conditions cause barrel expansion, erosion, and possible gas leakage from the base to the head of the projectile which cut the predicted muzzle velocities to half or a third of the lossless calculated values. However, in the case of a shock-tube operation these difficulties are minimized or eliminated and the possibilities of approaching Jovian reentry velocities are encouraging. In a recent run using about 100 g of explosive PETN and 400 psi $2H_2 + O_2$ a shock mach number $M_s \sim 60$ was obtained in air at an initial pressure of 1 torr in 1.0 in dia shock tube channel. In addition, the use of focused, explosive-driven implosion waves may have many other physical and technological applications.

PRECEDING PAGE BLANK NOT FILMED

hypervelocity launcher
shock tube

vii

NOTATION

e   specific internal energy

m   mass per steradian

p   pressure

q   artificial viscosity pressure

Q   specific energy source (or loss)

R   radial distance

R_O initial position of a Lagrangian surface

ρ gas density

t   time

T   temperature

u   particle velocity

v   specific volume

INTRODUCTION

A need still exists today to study hypervelocity impact up to 73 km/sec (the possible meteoroid impact limit in our solar system) and to conduct gasdynamic simulation up to 50 km/sec (the entry velocity of Jupiter in planetary explorations).

Although much effort has been expended on hypervelocity launchers over the past two decades, significant models have not been launched much over 10 km/sec (only the beginning of the desired range of interest for impact studies). Similarly, uniform, shock-heated test regions of significant duration in shock tubes are still only somewhat greater than 10 km/sec (far short of the desired velocities).

In order to assist in overcoming these velocity plateaus, it was felt that other means than driving launchers and shock tubes by planar-shock compression and heating must be found. The use of implosion waves for spherical-shock compression and heating appeared to offer unique possibilities, as ideally the pressures and temperatures at the implosion focus are unlimited. In practice, however, transport coefficients limit the gas properties to finite but still very large values, and the concept looked very attractive.

In order to verify the possibilities a facility was built (Reference 1), as shown in Figures 1 and 2. It consists basically of a hemispherical cavity, 8-in dia, in a massive steel block (Figure 3), which is covered by a heavy instrumentation plate, both fastened by a massive threaded locknut. A 0.22 calibre gun barrel (or shock tube) is attached at the centre of the instrumentation plate and it is then fastened to the hypervelocity launcher range (Figures 4 and 5).

The operation of this facility is based on generating a detonation in a stoichiometric hydrogen-oxygen mixture at the geometric centre of the major diameter of the hemisphere by using a fine, short, exploding copper wire as an initiator. The hemispherical front moves towards the periphery (Figure 6) and reflects from a shell of explosive, which is situated there. The impulsively and simultaneously initiated explosive shell drives an implosion into the preheated and compressed hydrogen-oxygen products and reflects from the origin leaving a pocket of gas at extreme pressures and temperatures that can be used to drive a projectile in a launcher barrel or a shock wave in a channel.

Initially a primary explosive, lead azide, was used. Subsequently, for reasons of safety, a secondary explosive, PETN, was found to be the most suitable from among many that were tried (Reference 2). Little encouragement was received from professional researchers in explosives that PETN could be initiated by a gaseous detonation. Nevertheless, the method proved very successful in generating stable, focused implosions. To date much is still to be learned why and how explosives detonate, especially when surface initiation as noted above is used.

Subsequently, a 24-in dia hemispherical driving chamber was designed for a 1-in dia barrel to launch single calibre plastic cylinders weighing 13 g and capable of having sensors with telemetred data (References 3 and 4). The design utilized the analyses of References 5, 6, and 7. The cost of such a facility was estimated at $175,000, and was not built owing to a lack of funds. Instead

two, one-third scale launchers were developed and improved (Mark II and Mark III, Figures 7 and 8) and the drawings of the 24 in dia facility were modified to incorporate the experience gained from the experimental investigations. An exploded view showing the details of the construction of the 8 in dia or 24 in dia launcher appears in Figure 9. It is seen that the basic design change was the elimination of the lock nut and its replacement by a 32-bolt fastening in order to allow the use of much greater weights of explosive and ease of operation as the lock nut was prone to galling.

Figure 10 shows a perspective view of the 24 in dia launcher (Mark II— the drawings were subsequently modified for the Mark III launcher). The overall dimensions and weights appear in Figure 11. This figure also shows the special hydraulic bolt-tensioner that would be required to prestretch the bolts before a run to ensure an appropriate load distribution when the explosive liner was initiated. The blast tank to trap the explosive gases before the projectile enters the range is also shown.

Scientifically, the project has been very successful as a means of investigating spherical deflagrations and detonations (References 8 to 10), the surface initiation of primary and secondary explosives in planar and spherical geometries (References 2 and 11), the properties of detonation-driven implosions for launchers and shock tubes (References 2 and 12 to 16) and a variety of reviews and analyses (References 17 to 32) associated with the facilities.

As a launcher this unique device has only been partially successful. This arises from the fact that a light, driver gas at modest pressures and temperatures (a few kilobar and a few thousand degrees Kelvin held for milliseconds) is a necessary requirement to launch projectiles intact that are made of present day light materials such as lexan, magnesium, aluminum, or titanium. Whereas, the present facility can generate pressures in the many hundreds of kilobars and tens of thousands of degrees Kelvin for very short times (in the microsecond regime) through the implosion process. When such conditions prevail at the base of a projectile, the material spalls and breaks up (accelerations of 10^{10}g's are possible). Furthermore, the erosion caused by such a driver gas would tend to turn it from an effective, light driver to an inefficient metal vapour (Reference 34). The resultant barrel expansion also would reduce the projectile base pressure and the final muzzle velocity. For example, in a recent run a 0.278 g titanium projectile was launched by 400 psi $2H_2 + O_2$ and 143 g PETN. It attained a velocity of 13,500 ft/sec. The projectile was moved 3.0 in inside the barrel to reduce the effective implosion pressures. On weighing the barrel after the run it was found that 45 g has been eroded away, that is, nearly 160-fold the weight of the projectile or 2.3-fold the weight of the hydrogen-oxygen driver gas (19.8 g). Roughly speaking, half of the predicted velocities are attained. However, as a result of the very high pressures and densities (Reference 35) analysis indicates that very high velocities could still be obtained if the projectile integrity was maintained and if barrel expansion and leakage from the base to the front of the projectile did not occur. Consequently, the question as to whether or not the calculated velocities of about 50,000 ft/sec can ever be achieved in this type of facility cannot be answered unequivocally without further development work.

An additional difficulty arises from the fact that a perfectly focused implosion can only be produced about 50% of the time. This may be mainly due to an uneven (density, geometry) PETN shell. An offset implosion makes for

irregular base pressure distributions and can lead to damage of the launcher components (References 4 and 15).

In case of the shock tube operation using a 1.0-in dia channel, the projectile integrity problem and that of a defocused implosion are eliminated. Consequently, improved performance can be expected. Recent results have shown that using a 400 psi $2H_2 + O_2$ and 96.5 g PETN driving combination a shock velocity of 62,000 ft/sec was obtained which was still accelerating a few feet from the diaphragm. Analysis has shown that shock velocities of 100,000 ft/sec should be possible with uniform flow of reasonable duration. This problem is presently being investigated. Such a possibility would make the implosion shock-tube driver into an important device for investigating planetary entry such as Jupiter, at 160,000 ft/sec. Undoubtedly, many other uses can be found for utilizing controlled implosions in a safe and resusable facility.

2. Analytical Considerations

The operation of the UTIAS Implosion-Driven Hypervelocity Launcher or Shock Tube was described in the foregoing, as shown in Figure 6.

The physical conditions and waves which are induced by this operation may be determined by solving the set of nonlinear partial differential equations of mass, momentum, energy, and state for the gas mixture(s) and explosive as given below, in Langrangian form,

$$\text{mass:} \quad \frac{1}{\rho} = v = \frac{1}{3} \frac{\partial R^3}{\partial m} \tag{1}$$

$$\text{momentum:} \quad \frac{\partial u}{\partial t} = -R^2 \frac{\partial}{\partial m} (p + q) \tag{2}$$

$$\text{energy:} \quad \frac{\partial e}{\partial t} = -(p + q) \frac{\partial v}{\partial t} + Q \tag{3}$$

$$\text{state:} \quad e = e (T,v), \quad p = p(T,v) \tag{4}$$

$$\text{or}$$

$$p = p(e,v), \quad T = T(e,v)$$

$$u = \frac{\partial R}{\partial t} \tag{5}$$

where $m = \frac{1}{3} \rho_1 R_o^3$

ρ = gas density
ρ_1 = initial gas density,
R_o = initial position of a Langrangian surface,

u = particle velocity,
v = specific volume,
R = radial distance,
p = pressure,

q = artificial viscosity pressure,   Q = specific energy source (or loss) rate
e = specific internal energy,   m = mass per stearadian,
T = temperature,   t = time.

The set of equations is solved by numerically integrating a set of corresponding
finite difference equations, using the artificial-viscosity technique, subject
to prescribed initial and boundary conditions (References 35, 36, 37, 38, 5, 6,
and 13). Some of the first results obtained by Brode (Reference 37) are shown
in Figures 12 to 15.

Brode did a detonation wave computation for $2H_2 + O_2 + 7He$ treated as a
perfect gas ($\gamma = 5/3$), which was originally thought as a possible (mainly-
monatomic) gas mixture for driving the projectile. The wave system in the (r,t)
plane is shown in Figure 12. It is seen that the detonation wave initially
moves at constant velocity and then it reflects from the periphery and the
origin (at ∿50 μsec). It accelerates as it approaches the origin and decelerates
as it moves away, but the net cycle time is practically constant. It can be
seen from Figure 13a that substantial pressures occur at the points of ref-
lection R = 0, at the implosion reflection, and R ≃ 10 cm, at the periphery.
The same remarks apply to the temperature shown in Figure 13b. Figure 14
shows the variation of pressure for a 16 in dia, rather than the 8 in dia chamber
actually constructed, as a function of radius for times ranging from 49.38 μsec
after the detonation wave (D) is instantly formed at the center of the 16 in
dia hemisphere (the actual 8 in cavity would give pressures and temperatures
greater than those shown for the same initial gas mixture and 0.1 in thick ex-
plosive liner owing to the higher energy density). At 49.38 μsec the
detonation wave hits the explosive. (TNT was used as a model since its pro-
perties are well known; the gas energy is 6.71 K cal; the ratio of explosive
to gas energy is 19.5.) The implosion wave (S) reaches the origin at about
67 μsec and reflects. (The detonation wave, implosion wave, and explosion
wave have spread transition fronts resulting from the use of artificial
viscosity in the numerical integrations. These can be made sharp by using
more zones in the computations, at greater expense, or can be arbitrarily
drawn sharp at the point where the artificial viscosity is a maximum.) It
can be seen that peak pressures of about 1/4 million psi can be achieved
even under these relatively mild initial conditions. The peaks achieve
asymptotic values for fine-mesh zones.

Figure 15 shows a similar plot of the temperature in the launcher com-
bustion chamber for the same times. The contact surface between the hot, dis-
sociated, and ionized gases, consisting mainly of helium, and the relatively
cool (about 1000°K) TNT products, is clearly indicated in this figure. Again,
temperatures of about 1/4 million degrees Kelvin are achieved.

Some of the results of this program appear in Figure 16. Figure 16a
shows the (x,t)-plane wave diagram of one of the cases that was run experi-
mentally by Flagg (Reference 2), that is, 200 psi of $2H_2 + O_2$, a 200 g PETN
shell, and a 5/16 in dia single-calibre, polyethylene projectile weighing 356 mg.
It is seen that the detonation wave (D) starts at the origin (here taken as
x = 10 cm) and races to the periphery (x = 0) at 2.9 km/sec, where it reflects
from the inner surface and detonates the PETN. The detonation wave races through
the explosive-gas to driver-gas contact surface, overtaking the reflected
detonation wave to form a very strong shock wave moving at 8 km/sec. This
shock hits the projectile at about 54 μsec and accelerates it to 12 km/sec.

4

The shock reflects from the base of the projectile, refracts at the contact surface and the reflected shock wave from the refraction process overtakes the projectile at 110 μsec and boosts its velocity to about 14 km/sec. The next overtaking shock wave, although travelling at 9 km/sec, no longer is able to overtake the projectile. Details of the other wave interactions are also shown. It is of interest to note that although the gas is compressed about 8-fold and the contact surface comes within 1.2 cm of the orifice, the explosive gas never leaves the hemispherical chamber during the launching period. That is, the compressed driver gas accelerates the projectile and during this period only about 2.4 g of the original mass of 12 g of driver gas has flowed from the chamber into the barrel. That is, the mass of gas to projectile mass used in accelerating it is about 7-fold. During the next cycle (150 μsec) the contact surface is even further from the origin (2.5 cm). Figure 16b shows the corresponding pressure and temperature at the base of the projectile as a function of time. In this case a diaphragm was not used behind the projectile. Consequently, it can be seen to accelerate gradually between 10 and 52 μsec to 55 m/sec and then very sharply to about 12 km/sec as the implosion strikes and is reflected. The peak pressure reaches 2×10^5 atm or an acceleration of about 3×10^8 g's. The peak temperature reaches about 37,000°K. The overtaking of the projectile by a second shock at about 110 μsec further accelerates the projectile to a final muzzle velocity of about 13.6 km/sec.

Figure 16c covers the runs that were performed by Flagg using PETN. Three main cases were calculated. In all cases 200 psi, $2H_2 + O_2$ and single calibre 5/16 in dia projectiles were used. In Case 1 the projectile was made of polyethylene and weighed 356 mg and 200 g PETN was used to drive it; in Case 2 the explosive weight was decreased to 100 g; Case 3 was similar to Case 2 except the projectile was made of magnesium, thereby doubling the density and giving a weight of 712 mg.

It can be seen that the lighter projectiles achieve a higher velocity up to 50 μsec (no diaphragm) and then they are all very rapidly accelerated in a few microseconds to nearly their maximum muzzle velocity for a 5 ft barrel. In Case 1, this velocity is about 14 km/sec, Case 2, 10 km/sec, and in Case 3, 7 km/sec, that is by doubling the explosive charge the velocity goes up nearly as the square root of the explosive energy and by doubling the mass of the projectile the velocity is decreased as the square root of the projectile mass.

Sevray (Reference 5) considered some of the initial conditions that were treated by Brode for the UTIAS implosion-driven hypervelocity launcher. This work is an extension of Brode's analysis to include the launching of the projectile. Essentially, Equations 1 to 5 are solved subject to the appropriate initial and boundary conditions and equations of state for the gas and explosive. This procedure has great merit in that the equations of motion are solved numerically for the entire system. However, care must be taken to use a sufficient number of physical zones to ensure asymptotically correct results, as noted previously. The physics can be extracted from the results as Flagg has done. It is only a first step in what is hoped will be a continuing improvement in the analytical work, which will account for interface instabilities, and radiative, ablative, frictional, conductive and other losses (References 34, 35).

Sevray also optimized the operation of the 8 in dia launcher by considering the effects of explosive shell thickness, initial pressure and

5

projectile mass (Reference 5). In addition, he also explored the effect of large chamber size and a 1.0 in dia barrel. Some of his results are summarized in Figures 17 to 20. Figure 17 shows that the explosive thickness determines whether a single pressure pulse or a double pressure pulse strikes the base of the projectile. If the explosive is thin to moderately thick, then the reflected gaseous detonation and the reflected explosive detonation combine to form a single implosion before striking the projectile base. If the explosive is too thick then they both strike the base in sequence, as shown. The net result for a fixed projectile (5/16 in dia, 0.356 g) of such impulses on a final velocity is a 5 ft barrel for different initial pressures of $2H_2 + O_2$ and weight (thickness) of PETN is shown in Figure 18. It is seen that beyond 400 g PETN (a thickness of about 0.1 chamber radius), the muzzle velocity falls. As expected, it increases with decreasing initial pressure due to the increasing compression and heating of the hydrogen-oxygen driver gas.

Figure 19 shows that the optimum conditions for a 8 in dia chamber, 0.22 calibre plastic projectile (0.13 g), is to use 200 psi $2H_2 + O_2$ and 400 g PETN, giving a muzzle velocity of over 60,000 ft/sec. In addition, Figure 20 shows that for a 30 in dia chamber, 1.0 calibre projectile (13 g) the optimum initial conditions are 200 psi $2H_2 + O_2$ and 18.5 kg PETN (0.588 g/cc, 1.255 kcal/g), yielding a velocity of about 45,000 ft/sec. As noted in the foregoing Introduction, very significant ablation and barrel expansion occur during a run, consequently, the calculated results, which were obtained by using a lossless (no friction, heat transfer, or ablation) and structurally rigid analysis are too idealized.

In order to design the Mark II and Mark III launchers, it was necessary to calculate the pressure at the periphery where the explosive shell contacts the metal cavity (Reference 6). Figure 21 shows such a history for a 30 in dia cavity and a PETN shell of 25 kg (the optimum case considered during the design phase (it was later switched to a 24 in dia cavity to save costs). The explosive detonation wave arrives at about 100 μsec after initiation of the gaseous detonation by the exploding wire. The pulse reaches a pressure of about 5.8×10^4 bars and decays to about 1.1×10^3 bars at 300 μsec. The reflected shock arrives at the wall at this time and raises the pressure to 1.35×10^4 bars. After this time a gradual decay of peaks and valleys occurs. Such pulses would induce compressive and unloading waves in the steel chamber block that could give rise to spall problems. As shown in Reference 6, by using a higher loading density PETN (1.5 g/cc, 1.415 kcal/g) it is possible to reach peak pressures an order of magnitude greater and calculated velocities of 108,000 ft/sec, but correspondingly greater (by an order) projectile base pressures and wall pressures.

Figure 22 shows the total force on the breechblock with time for the design case noted above. When the chamber is loaded with 200 psi $2H_2 + O_2$ a minimum load of 1.42×10^5 pounds occurs. At 80 μsec the load increases to 5×10^5 pounds owing to the gaseous donation pressure. At that time the explosive is initiated and a load of 3.5×10^7 pounds is achieved at 100 μsec. Subsequently the load rises to 1.5×10^8 pounds at 200 μsec as the reflected and refracted implosion wave from the contact surface arrives. Later on the waves decay and at times as long as 4,600 μsec, the load is 6×10^7 pounds.

In order to get an insight into the elastic-plastic wave propagation in the chamber resulting from these loads, Garg and Graf (Reference 7) did

6

some independent analyses. Results showing the displacement of the 30 in dia cavity as a function of time appears in Figure 23. An attempt was made to verify the data using strain gauges. Unfortunately, the work was not completed. Figure 24 shows a typical result from Reference 7, on the propagation of the elastic wave, the plastic wave and the unloading tension wave (right to left, respectively), as they develop and decay with time. The latter two waves travel with the same plastic wave velocity. Structural design based on such dynamic concepts is still in its infancy and much work remains to be done in this area.

In addition to the above study of materials under shock loading, Graf (Reference 39) is presently investigating analytically and experimentally some of the causes of projectile failure in the UTIAS implosion driven launchers. His investigations are addressed to the questions why and how projectiles fail when subjected to the extreme base pressures, temperatures, and densities existing in this facility. It is not envisaged that projectile materials (laminations, composites, or fibres) can be designed, at this stage, to withstand the extreme gasdynamic conditions that cause projectile break up.

To overcome the difficulties with projectile integrity, defocused implosions, and to investigate the limit of a massless projectile (the shock tube case) analytical and experimental work was initiated by Poinssot (Reference 13) and is being continued by Chan (Reference 40). Despite some difficulties at the origin in running the computer program to solve the limiting case when the projectile mass goes to zero, which have as yet not been resolved completely, some worthwhile results have been obtained for the shock tube mode. Figure 25 shows the time-distance diagram for a practical set of initial conditions. (Unlike Sevray, Reference 5, Poinssot did not run an optimization program for the shock-tube case.) It is seen that a shock velocity of 32.8 km/sec or a shock Mach number of 95 is produced in air. (A recent run by Chan using about 100 g PETN produced a shock velocity of 19 km/sec, making the above result quite credible.) It is of interest to note that the computed shock wave does not appear to decay. In addition, the computed pressure profiles (Figure 26) show a uniform flow (not a decaying blast wave type of profile) behind the shock wave. For example, at $t = 407$ μsec a pocket of hot gas 200 cm long (or of 50 μsec duration) is available for testing purposes in an 1100 cm channel. Again, this is a lossless calculation and some attenuation can be expected (in fact, for a 1 in dia channel the results look very promising).

3.   Experimental Results

3.1 Spherical Deflagration and Detonation Waves

The first investigation in the Mark I launcher was made by Benoit (Reference 8). It consisted of an analytical and experimental study of spherical deflagration of stoichiometric mixtures of hydrogen-oxygen diluted with hydrogen or helium. A considerable number of runs was made using initial pressures $75 < p_1 < 1000$ psi at room temperatures and various dilutions ignited by a spark or crimped wire. Detonation limits, pressure histories, thin-film surface temperature records, ionization-probe records, and total-light output from photodiodes were obtained. It is worth noting that the measurements were made in the "interior" of the spherical combustion process, at three radii at angles of 120° or six radii at angles of 60° with distances from the centre of 1 7/8 in and 3 3/4 in giving 6 or 12 measuring locations (Figure 27).

Previous measurements by other researchers were limited to points on the periphery or the centre.

Kistler type piezo-pressure gauges, SLM 605-B, in conjunction with type 652-B calibrators were used to measure pressures at various positions. Platinum, thin-film, heat-transfer gauges having glass, quartz, and magnesium-silicate-ceramic backings were used as wave detectors. These gauges were useful for measuring wave speeds and symmetry in deflagration runs but were readily destroyed in detonation experiments. Glow discharge gauges and Philips type OAP 12 photodiodes were also used to measure wave arrival and symmetry.

In the range $75 < p_1 < 1000$ psi using the present facility, it was found that smooth deflagrations took place with helium dilution of 3 to 15 moles in 3 moles (50 to 83% by volume) of the stoichiometric mixture. For dilutions of 3 moles of helium either deflagrating or detonating (transition limit) combustion took place, and below it detonation occurred. Mixtures with dilutions greater than 15 moles of helium could not be ignited. At 100 psi, 7 moles of excess hydrogen (a total of 90% hydrogen by volume) gave the transition limit and 10 moles (total of 92% by volume) gave the maximum dilution for ignition. Consequently, hydrogen diluted mixtures detonate much more readily (over twice the dilution) than helium (Figure 28).

A typical deflagrating combustion run is illustrated in Figure 29. The initial gaseous mixture was composed of 30 per cent of stoichiometric hydrogen-oxygen and 70 per cent of diluting helium, at room temperature (297°K) and at a pressure of 100 psi.

After ignition at the centre, C, the flame front moves radially towards the wall, W, at a low speed compressing the unburnt gas. The compression effects are transmitted in the vessel at the much higher characteristic velocity tending to equalize the pressure throughout the whole vessel, and preheating the unburnt gas. The combustion is accompanied by an expansion across the flame front and an appreciable temperature rise due to the heat released by the exo-thermic-reaction process. The expansion is readily visible at Station I in the early stage of the combustion process (F,I), but undetectable, on the oscillo-gram, at Station 0 when the combustion is near completion (F, 0). This sub-stantiates the classic assumptions usually made in connection with the deter-mination of burning velocity in a closed spherical vessel that the pressure is nearly constant throughout the vessel and that in spherical combustion as well, the pressure is nearly constant across the wave. The pressure record exhibits a maximum when the wave reaches the wall. Then the pressure decreases, almost linearly for a period of time comparable with the combustion time, as a result of the cooling of the system. The surface temperature record of Figure 29 clearly indicates that the increase in temperature in the unburnt gas due to adiabatic precompression (between ignition to F, on the figure) is negligible compared to the temperature jump across the wave. When the wave is passed, the heat transfer record shows a continuous increase until the flame has reached the wall and afterwards it either keeps increasing at a smaller rate or remains constant for some additional time.

The transition to detonation is illustrated on Figure 30. The wave first develops as a smooth deflagration. The wave is still in its deflagrating stage when it reaches Station I, as the heat transfer record indicates. Then some-where between Station I and the wall it develops into a detonation characterized

8

by sudden pressure increase and wave velocity of the order of 3 km/sec. This velocity is too high to be distinguishable between Stations I and 0 at the sweep times of Figure 30. The wave is reflected from the wall and the subsequent oscillatory nature of the traces is not due to mechanical vibrations, since indeed the heat transfer history recorded simultaneously shows the same overall frequency (about 530 cps, i.e., 190 μsec/cycle). Therefore, it is the image of the real flow process associated with the wave system model based on the idea that detonation in a spherical geometry would develop in a manner similar to planar detonations is advanced in Reference 11.

Figures 31 and 32 show final-to-initial pressure ratios measured in deflagrating combustion. In these figures the circles represent arithmetic mean values. The number of records used and the range of the values obtained are indicated for each ratio. The comparison of these values with the equilibrium final-to-initial pressure ratios computed for constant volume combustion (Reference 19) indicates discrepancies as high as 20 per cent. In fact, however, it was observed that the gauges were temperature sensitive, each in a different manner, and an appropriate correction factor was not evaluated.

The work of Benoit was extended by Watson (Reference 12). He showed that excellent agreement with the analysis of Benoit (Reference 20) was obtained on detonation velocities as a function of initial pressure and dilution (Figure 33). Unfortunately, because of the very hostile environment produced by detonation waves at high pressure, it was not possible at that time to use sensors to obtain physical profiles behind the detonation wave. Nevertheless, it is believed that these are new velocity results for spherical detonation waves in $2H_2 + O_2$ up to 500 psi initial pressures.

In order to get some photographic data of the gaseous detonation process in the hemispherical cavity Macpherson (Reference 25) substituted a 3 1/2 in thick lucite plate for the steel plate of the Mark I launcher. The lucite window was reinforced by two steel bars 2 1/2 in apart. The initial pressures of $2H_2 + O_2$ was kept in the range $175 < p_i < 400$ psi. The same type of copper wire (0.002 in dia x 0.063 long) was used as in an actual run. An image-converter framing camera was employed to photograph the luminous regions as shown in Figure 34. Some distortion of the photographs was caused by curvature and refraction through the lucite.

It is seen that the luminous fronts appear irregular, asymmetric and of uneven exposure and suggests the possibilities of varying time of arrival of the detonation wave at the periphery of the hemisphere and of uneven focussing on reflection. The Chapman-Jouguet detonation velocity was obtained after an initial period which varied in time and in area affected. Somewhat improved symmetry was obtained in going from initial mixture pressures of 200 psi to 400 psi. Below 200 psi the process appeared unreliable.

In assessing this work, it should be noted that the chamber running conditions were not exactly duplicated. It contradicts the work of Watson noted above where good agreement with theory for detonation velocities was obtained as low as 100 psi initial (Figure 33). It also contradicts the work of Chan (Reference 15), where he was able to get nearly perfectly centred implosions by paying attention to the method of admitting and mixing the gas. This could not have been achieved if the original detonation wave was asymmetric with respect to the origin. However, Macpherson's work resembles some of the

9

data reported in Reference 41, for low initial pressures, where it is shown that enough energy must be produced at the initiating source to produce an overdriven detonation that decays to the Chapman-Jouguet value if it is to be symmetrical. It may be concluded that a similar study on the exploding wire initiation would have to be done at the very high initial pressures used in the hemispherical chamber, where in fact greater stability and symmetry can be expected, in order to settle this question.

3.2 Surface Initiation of Solid Explosives by Gaseous Detonation Waves

The key to the operation of the hypervelocity launcher depends on the instantaneous and simultaneous initiation of the hemispherical shell of solid explosives by the oxygen-hydrogen detonation wave. Very little encouragement was received from explosives experts that this would be possible. The reason stems from the fact that it is still not known in detail how and why an explosive actually detonates under these conditions.

In order to study the initiation problem a much simpler, one-dimensional apparatus was built for this purpose rather than using the hemispherical chamber, as shown schematically in Figure 35, and photographically in Figure 36. In addition, only 1/60 of the amount of explosive is required. The chamber consists of three thick plates. The centre plate has a cylindrical cavity 1 1/2 in dia x 4 in long. The length corresponds to the radius of the hemispherical chamber radius for comparison purposes of the initiation work in both chambers. At one end of this cylinder there is space to take the explosive cup containing the test explosive (about 0.15 in thick x 1 1/2 in dia, 3.7 g at a density of 0.85 g/cm^3), and at the other end the cross-wire ignition for initiating the detonation wave in the hydrogen-oxygen mixture. Three ionization gauge stations (at the centre and ± 1 1/2 in) for measuring incident as well as reflected wave velocities can also be seen.

The work was started by Makomaski (Reference 11) who qualitatively inferred the occurrence of detonation from the deformation of the cup containing the explosive. The quantitative results were obtained by Flagg (Reference 2). During a run, the cross-wire (4 mil copper x 1.2 in long; a fraction of 135 joules x 6 kv of the capacitor bank is used, the rest is dissipated) is exploded to provide a planar detonation wave as quickly as possible. The incident wave speed is measured and provides a check on the gaseous mixture. The wave impinges on the explosive in the cup and the reflected wave speed indicates the consequence of the addition of this energy.

Figure 37 shows a time-distance plot of the initiation of stoichiometric hydrogen-oxygen as a function of initial pressure of the mixture. It can be seen that the detonation velocity (about 3 km/sec) is initially greater (overdriven) for the lower gas pressures because the energy input from the exploding wire is a noticeable fraction of the total energy per unit volume. The reflected wave accelerates as it moves into the rarefaction zone behind the initial detonation wave.

Figure 38 shows the effect of the lead azide explosives as a function of the energy per unit surface area of the explosive disc divided by the initial pressure (E_0/p_1). This is the correct energy parameter for energy release at a plane. It is seen that the highest reflected wave velocity is obtained for

10

the largest value of E_0/p_1. The runs at 3 atm show an instantaneous surface initiation of the lead azide, whereas the run at 2 atm shows a "delay" of about 4 μsec. The slower reflected shock trajectory from the $2H_2 + O_2$ run (dashed line) is shown for comparison. It should be noted that this "delay" is essentially composed of the slower reflected shock trajectory plus the overtaking blast wave when the explosive initiates. It only appears as a discontinuous delay due to the arbitrary backward projection of the reflected wave to the explosive surface.

Figure 39 shows a similar plot for PETN pressings of about 4 g. It is of interest to note that in all cases the initial pressure is high enough that the exploding-wire energy has no effect and the same detonation velocity (3.06 km/sec) is obtained. The initiation is instantaneous for the high-pressure run but there is a characteristic "delay" for the lower pressure runs.

Figure 40 has an (x,t) plane plot for Superfine PETN ($\rho=0.59$ g/cm^3). The results are quite similar for the 100 and 50 psi cases, except that in the latter case the delay exceeds 10 μsec. The $1/\sqrt{x}$ velocity decay predicted by planar blast wave theory is also observed. When the pressure was reduced to 25 psi the explosive did not detonate. The reflected wave is then just the one arising from the stoichiometric mixture, as the deflagrating explosive adds negligible energy over the time interval under consideration.

3.3 Production of Explosive-Driven Spherical Implosions

Although the data looked very promising for the one-dimensional planar wave initiation it was still necessary to show that the same results would apply to the spherical geometry of the hemispherical shell of explosive as the physical profiles of the initiating detonation waves are different in the two geometries.

It was known that, owing to the additional degrees of freedom to expand and quench, it would be much more difficult to initiate even gaseous spherical detonations than planar detonation waves. Consequently, although it was shown that 1 1/2 in dia discs of lead azide, PETN, and nitrocellulose will detonate when initiated by a planar detonation wave, it was not at all certain that this could be done in the 8 in dia hemispherical driving chamber, which contains about 60-fold the amount of explosive. Also the explosive shell is subjected to a spherical detonation wave with temperature and pressure profiles that are quite different from those of the corresponding planar wave profiles, as noted above. Nor was it possible to tell beforehand whether the hemispherical sheet of explosive would detonate simultaneously to produce stable, centred, explosive-driven implosions. Some of the basic questions regarding the stability of unconfined implosion waves and those generated using the present method in a finite sphere have not as yet received a detailed analysis. Nor are things too well known about the stability of the contact surface separating the dense explosive gas from the light hydrogen-oxygen driver gas under acceleration-deceleration profiles of short duration, which can have a significant influence on the conditions in the driver chamber. It was therefore necessary to show experimentally acceptable simultaneous initiation of the hemispherical explosive shell and subsequent stability of the implosion wave.

The construction of explosive hemispherical shells (8 in dia x 1/8 to 3/16 in thick) of lead azide and PETN is described in References 2, 33, 4 and 15. The explosive shells are bonded to metal shells and the package is then inserted as

a, complete unit into the hemispherical cavity (Figure 1). Lead, aluminum, copper and steel have been used for metal shells and so far the copper has proved the most satisfactory from the point of view of spinning, machining, and durability.

Flagg(Reference 2) has previously shown that by placing a copper "witness" plate (1 1/2 in dia x 0.5 in thick) where the gun barrel is normally held in place one could obtain on imprint of the implosion and thereby determine its stability and focusing properties. Figure 41 shows this very effectively for a gaseous detonation only, and when 88 g PETN are added. It is seen that excellent focusing and stability can be obtained. The pressures and temperatures generated by the implosion causing the copper to flow like a liquid are well illustrated. Unfortunately, not all runs (about 50%) were that good or repeatable when explosives were used, but were excellent (within 1 mm radius) for all gaseous detonations only, as noted previously. (Further details are given in Reference 15.) Similar experiences were encountered by Huni (Reference 42) in the study of imploding cylindrical detonations. A figure of one-in-six runs is mentioned as being a perfectly centred, focused implosion, whereas for the UTIAS exploding wire system with rapid mixing, Chan (Reference 15) found the centring to be 100% in gaseous-detonation implosions.

Defocused explosive-driven implosions and off-centred implosions were obtained more often (about 50%; the fact that the implosion had to refract at the explosive gas-hydrogen-oxygen contact surface did not help its stability or symmetry) resulting on several occasions in severe damage to the apparatus that took skillful machining to repair (Reference 15). Explosive runs also resulted in projectile breakup in trying to increase the weight of explosive to push the limits of muzzle velocity in this facility. In order to alleviate this problem, the projectile was placed about 2 to 3 in downstream from the centre of the hemisphere. It is seen from Figure 42 that pressures and temperatures were still so severe as to cause irreparable distortion and erosion. This is a major difficulty with the present launcher: too-high pressures and temperatures for too-little time. This problem will be discussed subsequently.

Further evidence on stability and focusing of implosions was provided by Roberts (Reference 10). He studied spectroscopically the temperature profiles for the reflection phase of a $2H_2 + O_2$ implosion. An (x,t) - plane diagram of such an implosion (Reference 23) appears in Figure 43, showing the phases of detonation, implosion (at about 90 μsec), and reflection from the periphery. Figure 44a shows the experimental arrangement using the Mark I launcher, a Hilger medium-quartz spectrography and a Strassheim photomultiplier attachment. A quartz window was inserted (like the copper witness plate) at the centre of the hemisphere (see Figure 45 for details). The neatly "drilled" quartz window following a centred implosion is shown in Figure 44 b, while Figure 44 c illustrates the spectacular process on a time integrated photograph.

Further evidence for centred implosions appears in Figure 46 b, showing the focusing process as seen through a TRW, image-converter camera. The image of the 1/2 in dia quartz window is progressively reduced, in step with the first implosion. Figure 46 a illustrates through a photomultiplier record the phases of ignition, detonation reflection from the periphery (liner), and the light pulse from the first implosion. It is worth noting that Roberts (Reference 10) did quantitative time-resolved temperature measurements of the

12

gaseous implosion phase, as shown in Figure 47, for 100 psi $2H_2 + O_2$. It is seen that he did not measure temperatures in excess of about 5000°K. This result is considerably less than that calculated by Brode (Reference 37, see Figure 13) but in much better agreement with the analysis of Elsenaar (Reference 23), owing to the averaging process that he used over an area equivalent to the projectile base, which yielded a reduced average temperature as compared with the peak temperature generated by a collapse to zero radius. Nevertheless, this is a surprisingly low result in view that the temperature behind a planar detonation at an initial pressure of 10 atm and temperature of 300°K, is already 4,200°K (Reference 21). It is of interest to note that temperatures of about 15,000°K are reported in Reference 42 for cylindrical implosions in oxygen-acetylene detonations at low initial pressures (200 torr).

From the foregoing it can be concluded that stable, focused implosions can be generated, in safety, and in a controlled manner by using spherical gaseous detonations to initiate a spherical shell of explosive in a facility of the type of developed at UTIAS. It was also noted that about 50% of the explosive-driven implosions were off-focus by varying degrees owing mainly perhaps to the non-simultaneous contact and initiation of the explosive shell arising from imperfections in geometry, thickness, and homogeniety. Perhaps, some of these may also have been caused by nonrepeatability of the exploding wire (although this is doubtful as 100% focusing was obtained using gaseous detonation runs only). These faults could be overcome by a "standardized" ignition unit and quality control of the explosive shells. To achieve simultaneous initiation, a light sensitive explosive such as silver acetylide-silver nitrate ($Ag_2C_2 \cdot AgNO_3$) was also unsuccessfully tried (Reference 15). It would have had the advantage not only of simultaneous initiation but also of driving an implosion into a pure, light gas such as hydrogen or helium. As can be seen, there are many areas here for research and development in the improvement of generating repeatable, centred, explosive-driven implosions in the laboratory.

3.4 Launcher Operation

The first explosive-driven projectile runs were made by Flagg (Reference 2) following a preliminary investigation by Watson (Reference 13) on gaseous detonation driven projectile runs. Watson showed that the best results were obtained by using stoichiometric oxygen-hydrogen mixture (Figure 48). This result is in agreement with the fact that the "escape speed" has then the highest value (Reference 33), whether the gases are considered frozen or in equilibrium. In the range of $2H_2 + O_2$ initial pressures of $100 < p_i < 500$ psi, he obtained muzzle velocities of $4000 < u < 8000$ ft/sec for 126 mg plastic projectiles. These results are about half the values calculated by Sevray (Reference 5), as illustrated in Figure 49. Figure 49 (a) shows Sevray's results for one of Watson's detonation runs for 200 psi, $2H_2 + O_2$, using a 0.22 in dia polyethylene projectile, 1 calibre long, weighing 126 mg ($\rho=0.92$ gm/cm^3). The pressures and temperatures at the base of the projectile along with the projectile velocities are plotted as a function of time or distance along the barrel. Although the detonation velocity for t = 0 has the correct value (3 km/sec), the pressure ratio and the absolute temperature are lower as expected for spherical detonation waves, than the values given by Benoit (Reference 21), for planar detonations. There are also some oscillations at the base of the projectile resulting from the interior flow, and at about 90 μsec the reflected detonation wave reaches the projectile base causing the temperature there to reach 5500°K

13

and the pressure 4000 atm. The diaphragm behind which the projectile is placed is then ruptured and the projectile is accelerated to 600 m/sec. The peak acceleration is about 8×10^6 g's. Two additional decaying peak pressures occur at 210 μsec and 290 μsec which successively accelerate the projectile to its final velocity of 2.7 km/sec in about 600 μsec over 3 ft of barrel. The average temperature stays at about 3000°K. During this period about 0.25 gm of the original 15.5 g of gas has left the chamber.

It is also of interest to note that only about 1/4% of the gas energy is coupled to the projectile and this indicates the low overall efficiency of hypervelocity launchers. If some improved method of coupling could be produced, then the muzzle velocities would be correspondingly increased.

The actual value of the muzzle velocity obtained by Watson was about 2 km/sec. The experimental and computed runs appear on Figure 49 (b), and it is seen that, whereas the computed values show nearly a linear increase of muzzle velocity with initial pressure of the stoichiometric mixture, the experimental values however show an increase that becomes progressively smaller than predicted. For example, at 500 psi, the computed muzzle velocity is 13,000 ft/sec and the experimental value was about 7700 ft/sec. This indicates that losses are becoming more significant with increasing driving pressure and temperature. Even though the peak base pressures (accelerations) are predicted to be very large, the projectiles did come out intact and it shows that the polyethylene projectile was able to withstand accelerations of millions of g's perhaps, without disintegrating.

Elsenaar (Reference 14) further pursued the gaseous detonation driven runs by investigating the motion of the projectile using microwave techniques. It was reasoned that if an accurate measurement of the trajectory could be obtained then the projectile acceleration would be determined and knowing the projectile mass the extremely large base pressure could be found in a very direct and attractive way. Furthermore, it was hoped to see when and where the projectile broke up under explosive loading.

The experimental microwave system is shown in Figure 50. It consists of a 34 Gc source (15mw/Klystron) in rectangular waveguides coupled to 5/16 in dia x 5 ft long launcher barrels, giving a guide wavelength of 11.3 mm. The frequency shift resulting from the moving projectile is displayed on an oscilloscope. Figure 51 shows some of the velocity profiles obtained for a single-calibre 5/16 in dia magnesium projectile weighing 0.67 g, using 400 psi $2H_2 + O_2$, and their repeatability. It is seen that the projectile is accelerated by the first implosion and its reflections. The largest velocity increment follows the first implosion and then decreases owing to the motion of the projectile and the consequent attenuation and overtaking of subsequent reflection inside the barrel. By the end of about 350 μsec most of the acceleration has already occurred. It takes another 1000 μsec before the projectile leaves the barrel. Elsenaar modified and made use of the existing computer program (Reference 23) to compare the projectile motion for small times (< 150μsec), when the influence of the change in geometry at the origin from the hemispherical driving chamber to the cylindrical barrel is still small. From Figure 52 it is seen that the agreement with the microwave measurements shown in Figure 51 for the first cycle is very satisfactory. Elsenaar also showed that the temperature profile measured by Roberts was in good agreement with his calculations for the first implosion (Figure 47). The fact that higher velocities than ideal are obtained

14

may be due to the fact that the numerical calculations have not converged to the final values or that the physical conditions such as base pressure duration may be higher than calculated. The fact that only about half the predicted muzzle velocity is obtained shows that although the initial motion is nearly lossless, as time goes on viscous, ablative, and gas leakage losses reduce the expected performance.

Following the gaseous detonation on runs made by Watson (Reference 12) the work was extended by Flagg (Reference 2) to explosives using initially lead azide (PbN_6). This primary explosive is hazardous to use even in the supposedly safe, wet (water slurry) state. Consequently, it was abandoned in favour of PETN, which is a safe, secondary explosive requiring much higher pressures of $2H_2 + O_2$ to initiate (see Figures 37 to 40).

Figure 53 is a performance analysis made by Flagg of actual and predicted velocities for gas runs and lead azide explosive runs. This analysis was done before the computer program for the full equations of motion and state using the artificial viscosity technique (Equations 1 to 5) became available. The abscissa shows the projectile velocity of a 0.22 in dia, single-calibre poly-ethylene cylinder projectile in a 5 ft barrel and its kinetic energy (130 mg). The ordinate shows the total energy release of gas plus explosives or gas alone, where applicable. Four oblique lines give the velocities that would be obtained if there was 1/10 to 100% conversion of chemical to directed energy.

In his semi-empirical-analytical analysis Flagg based his anchor point (8000 ft/sec) on the gaseous launchings of Watson (open circles) to predict the performance increases. However, in Flagg's analysis, because of the choice of the anchor point, the gas runs agree reasonably well even at the end points. The lead azide runs, initiated by 100 psi $2H_2 + O_2$, are also in reasonable agreement with the predicted curve when the driving energy is based on gas plus explosive energy. However, if only the explosive energy is used, then the lead azide runs have a slope which approaches the asymptotic value of the predicted curve. It is seen that the predictions are apparently that initially the rate of change of velocity with explosive is very large (100 g of lead azide will initially increase the predicted velocity from 3000 ft/sec to 15,000 ft/sec) but not so later on, where the velocity varies as the square root of the energy. As Sevray has shown (Figure 18) the performance in fact decreases as the ex-plosive thickness is increased beyond the optimum value of approximately 1/10 of the hemisphere radius and these curves when accurately computed do show this feature (Reference 6).

The efficiency (ratio of projectile energy to chemical energy) of the present runs appears to be between 1/10 and 1%. This figure is of academic interest to some extent. Although this and other devices which produce hyper-velocities are very inefficient ($\sim 1\%$), this would be a small price to pay for achieving truly large hypervelocities. It shows that the energy coupling process is very poor, as noted previously, and if some method could be developed to improve this coupling by sustained base-pressures over long periods very large increases in velocities could be obtained. A maximum of 15,000 ft/sec was obtained using an explosive shell 0.1 in thick weighing 200 g. On the average, the agreement with the analysis is $\sim 50\%$.

It is also of importance to note that the velocity goes up rapidly when comparing the total driving energy of gas or gas plus explosive. That is, it

is the explosive-driven implosion which gives this unique device the large
predicted performance. The actual runs, although only half as effective,
nevertheless, bear this out quite clearly for the lead azide runs.

Elsenaar has collected about 35 runs, as shown on Figure 54, for PETN
driven projectiles (200 psi $2H_2 + O_2$ and 100 ± 30 g PETN) having various
weights (lexan, magnesium and titanium were progressively used to avoid pro-
jectile failure) in 3/16, 0.22 and 5/16 in dia barrels with lengths between
5 and 10 ft. Although the initial conditions are not precisely duplicated,
the results do illustrate the point that the gas runs and explosive runs differ
in some very important aspects. The gas runs do not have a very large decay
with projectile mass, which indicates that the multiple-reflected implosions
assist in progressively increasing the final velocity. However, the explosive
runs depend on the first implosion to attain most of the velocity (Figures 16
and 25), as the subsequent reflections are too slow to catch up. Even when
they are not very effective after they have undergone attentuation in the barrel.
For this reason the velocity after the first implosion for the gas case is
also shown to enable a reasonable comparison. It is seen that the explosive
is several times more effective initially, although finally, for heavier pro-
jectiles, the two methods of driving are not so different in their muzzle
velocities. When this data is compared with conventional launchers shown in
Figure 55 (References 43 and 44) it is seen that at the 0.1 g range only about
half the performance is obtained in the UTIAS launcher and is worse at the 1.7 g
range. As noted in the Introduction, the very large ablation, erosion (Figure
42), and barrel expansion caused by the extreme pressures and temperatures in
the UTIAS facilities may well be the cause of the degradation in performance
compared with the optimistic predictions of the lossless calculations.

Elsenaar (Reference 14) also showed that it was not possible to use the
microwave system owing to gas leakage around the projectile that generated
an ionizing shock of high velocity that reflected the microwaves rather than
the projectile. Pressures are so great around the origin that the barrel itself
is quickly spread (Reference 45) and when coupled with the erosion (see Reference
15 for further details) there are possibilities for leakage which can rapidly
degrade the launcher performance.

In order to reduce some of the serious structural problems caused by
defocused explosive-driven implosions it was decided to employ a conical ($\theta = 15°$)
(protector) liner plate, as shown in Figure 56 (see References 4 and 15 for
further details). In addition, to protect the projectile from the enormous
pressures and temperatures at the origin, it was recessed a distance, L_r, up
to 3 in downstream of the origin. The entrance to the new location of the
projectile was also flared at an angle α of 5 or 10 degrees. An analysis
(Reference 15) of these geometrical conditions is shown in Figure 57. Case 1
is the standard hemispherical drive without recess or flare using 400 psi $2H_2 +$
O_2 and 100 g PETN and a 0.292 g, half-calibre, titanium projectile in a 0.22
calibre barrel. Case 2 shows the performance when only a 15° conical plate
is used thereby reducing the weight of explosive. In both cases the lossless
analysis predicts a velocity of 8 km/sec. Cases 3 and 4 maintain the same
conical plate and now have a recess of 3 in and a flare of 5 or 10 degrees.
It is seen that recessing the projectile has a beneficial effect on velocity
which is now over 10 km/sec. The flare angle does not appear to matter in
this range. In practice it has been found that recessing prevents projectile
breakup by reducing the intense base-pressure pulse thereby resulting in higher
muzzle velocities.

16

Figure 58 shows a similar analysis and comparison with actual runs in the Mark III, 8 in dia, 0.22 calibre launcher. Numerical solutions at discrete points are shown for a purely hemispherical cavity and for a 15-degree conical plate and a 3-in recess with a 5 and 10-degree flare. The actual velocities obtained for half-calibre, 0.28 g titanium projectile, 0.22 in dia with centred and off-centre implosions appear on the figure for 400 psi $2H_2 + O_2$ and PETN weights between 75 and 175 g. It is seen that about one-third of the predicted lossless, muzzle velocities are obtained. It is worth noting that the weight of explosive is far short of the optimum required to produce muzzle velocities of about 40,000 ft/sec (400 of PETN, 400 psi $2H_2 + O_2$, Reference 5).

A sectioned barrel after such a run appears in Figure 59, and is compared with a sketch of the original barrel dimensions. About 45 g of barrel material was eroded in this run, that is, about 160-fold greater than the projectile mass. The regions of high pressure at the flared entrance and at the position of the base of the projectile are readily seen. This and subsequent barrel expansion rapidly decay the driving pressure. (Reference 45). In addition, leakage to the head of the projectile may also occur. The erosion produces a very dense driving gas. All of these factors can combine to produce severe losses and a drastic reduction in performance.

Figure 60 shows a comparison made by Chan (Reference 15) using Flagg's program (Reference 6) with the results of Brode (Reference 35) for the scaled-up version of the 24 in dia, Mark III, UTIAS Impolosion-Driven Hypervelocity Launcher. It is seen that the lossless calculations by both groups are approximately the same, as expected. However, the improved equation of state (EOS) results including ablative losses (Reference 34) used by Brode actually show a better performance up to 3 m of barrel length (indicating the use of short barrels). This surprising result comes about from the increased pressure and density ($\sim$ 1 megabar, 2g/cc) arising from the new equation of state for the driver gas. In view of the present results and those of Watson and co-workers (Reference 45) it is doubtful if such pressures could be maintained in the barrel long enough to yield the predicted performance in a 1 in dia barrel. It is true that stress gradients do not scale and are weaker in a larger projectile and larger launcher barrel (Reference 39) and projectile survival and performance would be improved. However, judging from the results of the one-third scale Mark III launcher noted above, it is doubtful if such performance is achievable without a lot of new, careful design and research.

The hypervelocity performance graph shown in Figure 55 has been re-plotted in Figure 61 to include some of the latest available data of very high performance from Physics International (Reference 45) and the best data obtained at UTIAS to date. It is seen that we are far short of the standard launcher performance, even though analytically we should be about as far to the right of the standard curves in performance as we actually are to the left of the curves. To date, the performance of the Physics International launchers is the most impressive in accelerating 2 g projectiles to 12.2 km/sec. However, as launchers they appear relatively complex to operate and have the disadvantage that they are destroyed after every run. Perhaps a new, simple approach is required to accelerate projectiles to very high velocities. It appears that the work of Titov and Fadeenko (Reference 46) may offer such a possibility for special applications using simple spherical projectiles.

3.5 Shock-Tube Mode

The difficulties encountered with off-focus implosions, barrel erosion and expansion, projectile integrity, and gas leakage from the base to the head of the projectile are largely overcome when the launcher is operated in the massless-projectile or shock-tube mode. For example, off-focus implosions within the diaphragm open-area of 1 in dia would not be significant. Whereas defocused implosion beyond that area, when explosive shells are used, may have an effect here as well. The analyses done by Poinssot (Reference 13) and illustrated in Figures 25 and 26 showed that the facility had promise as a shock tube and shock Mach numbers of 100 or more with uniform flow of reasonable duration (50 µsec) appeared possible. The numerical results are again based on lossless assumptions and they have the added difficulty of zoning around the origin arising from trying to match the very dense driver gas with the rarefied gas in the shock-tube channel. In addition, it was not possible to reach the shock-tube limit from the launcher analysis by letting the projectile mass go to zero. These numerical difficulties are presently being revaluated by Chan (Reference 40). Nevertheless, the results looked so promising that an exploratory investigation was made using a very impractically-small bore, launcher barrel as a shock-tube channel (References 13, 27).

It was not meant to be an extensive study of the performance of this type of shock tube. Rather, it was aimed to check the results of the computations and to give an estimate of the losses, as the computer code did not take account of them. However, this preliminary work has been extremely helpful in assessing the deficiencies of the code and in the design of a new 1.0 in (25 mm) dia shock tube that will not suffer from as many viscous effects.

The results were obtained in an 8 in dia chamber. The barrel was a stainless steel, high-pressure tube having a 5/16 in (8 mm) internal diameter. It was approximately 4 m long. A stainless-steel, scribed diaphragm, 0.015 in (0.4 mm) thick, previously calibrated, was used to separate the channel from the hemispherical driver near the origin.

The velocities of the shocks were measured using three different methods. Five ionization probes were placed along the barrel 14 in (36 cm) apart to detect the arrival of the ionization front. These were corroborated by using small optical windows and photomultipliers to detect the luminous front at the same stations. The agreement was excellent. Additional substantiating velocity data for the 400 psi case, as shown on Figure 62, were obtained with 34.4 Ghz (12 mm wave length) microwave Doppler system (Reference 14). The agreement was again satisfactory.

A summary of the experimental results that have been obtained to date appears in Figure 62. It shows the maximum average velocities and their decay over a distance from 10 to 225 cm using 200, 400 and 600 psi $2H_2 + O_2$ initial into a 1.0 torr air, without explosive liners. It is seen that maximum average velocities of 5.3, 8.2 and 13.7 km/sec, respectively, were obtained near the origin giving shock Mach numbers of $M_s \sim 6$, 24 and 40. The rate of decay of the shock was very high. For example, it drops from $M_s \sim 40$ to $M_s \sim 11$, in a distance of about 180 cm, or an average Mach number decay rate of approximately $\Delta M_s / \ell \sim 5/ft$. Such high rates of decay can be expected if we consider the very small diameter of the channel and its attendant viscous losses at the prevailing high shock Mach numbers, and a

18

detonation driver that relies on focused implosions on a small cross-section.

To overcome the difficulty caused by using a small-bore tube, a new shock-tube channel was designed by Chan (Reference 40), as shown in Figure 63. The 1.0 in dia shock tube channel consists of three, two-foot sections and one, one-foot section with observation windows that may be placed anywhere along the channel, as indicated. The scribed stainless-steel diaphragm is also shown in position in the hemispherical driving chamber. The end of the channel is fitted into the hypervelocity range tanks, which are evacuated. The ionization-gauge stations are also shown and other types of sensors and flow visualization techniques can be used. The actual driving chamber and part of the channel are shown in Figure 64.

Some of the preliminary results using a gaseous detonation implosion driver for 200, 600 and 800 psi initial pressure in the $2H_2 + O_2$ mixture appears in Figure 65. The shock velocity W_s is normalized by the maximum shock velocity and the distance is normalized by the hydraulic diameter. It is seen that a very modest attenuation results, which compares very well with the large 4 in x 7 in UTIAS Hypersonic Shock Tube (Reference 47). The 800 psi runs resulted in maximum shock velocities of 11.4 km/sec (37,500 ft/sec) as shown in Figure 66, which remained quite uniform over the test length of about 6 ft, as noted previously. The results for the 5/16 in dia channel obtained by Poinssot are also shown and the large attenuation is evident. Recent data obtained by Chan (Reference 40) using 96 g and 84 g PETN with 400 psi $2H_2 + O_2$ in the 1.0 in dia channel shows a shock wave velocity of 62,000 and 55,500 ft/sec, respectively. The shock wave was still accelerating over the 2 ft test length of channel. These preliminary results are most encouraging.

Figure 65 was compiled by Warren and Harris (Reference 48), and the UTIAS results and the data of Crowley and Glenn (Reference 34) on the Voitenko compressor have been added to bring the figure up to date. It is seen that the Voitenko compressor and the UTIAS data for the 5/16 in dia channel behave like the electromagnetic drivers shown in the figure, that is, like a decaying blast wave. The UTIAS gaseous-detonation-implosion drive has the characteristics of the implosion-jetting (Reference 45), electrical, piston, and combustion drives resulting in high shock Mach number and modest attenuation. Even with an 800 psi $2H_2 + O_2$ driver the UTIAS data is nearly as good as the explosive (implosion-jetting) drivers and better than most conventional methods. The UTIAS explosive-driven implosion generated shock waves appear to be off on a good start and it is hoped that they can reach the calculated result of 33 km/sec shown as an unattenuated horizontal line. Perhaps this line can be exceeded and Jovian re-entry velocities of 50 km/sec may yet be achieved.

It is worth noting that 1.0 g of explosive contains about 1100 cal or about 5000 joules of chemical energy. An explosive liner for the Mark II or Mark III 8 in dia Launcher usually contains from 100 to 500 g PETN. Consequently, energies from 1/2 to 2 1/2 megajoules are available to drive the shock wave. A large capacitor, with a short discharge time, delivering 5000 joules would cost about $2,000, or a total of one million dollars for 2 1/2 megajoules. By comparison the cost of an explosive package is only a few dollars (the explosive itself is worth a few cents) and is very safe to use in a reuseable facility of the type developed at UTIAS.

4. Discussions and Conclusions

It was noted that a need still exists to study hypervelocity impact up to 73 km/sec and to investigate gasdynamic entry simulation up to 50 km/sec.

The UTIAS implosion-driven hypervelocity launchers offered analytical possibilities of achieving projectile velocities of 20 km/sec. This has not been achieved in practice. Only a maximum velocity of 17,650 ft/sec (5.4 km/sec) was achieved for a 0.356 g plastic, single-calibre, 5/16 in. dia projectile that came out distorted. The basic difficulty stems from applying an enormous pulse (millions of psi) for very short duration (microseconds) (this is also typical of cylindrical-implosion launchers, see Reference 45, but they are not as intense) that causes projectile break-up, barrel distortion, erosion, and gas leakage. Consequently, to improve this concept technologically as a launcher, much work would have to be done on using less-explosive propellants in order to reduce the peak pressures and to increase the time of application at the projectile base. Perhaps this could be achieved using multilayered propellants with different detonation or burning velocities.

Laser initiation of the explosive-propellant packages would be desirable to ensure a well-focused implosion during every run through instantaneous, and simultaneous initiation of the explosive surface. The present exploding wire technique coupled with the surface initiation of the explosive shell by the gaseous detonation accomplishes this only 50% of the time.

A study of new materials using carbon, boron, or other fibres may be very helpful in providing light, high-strength projectiles. This would alleviate the projectile-integrity problem not only in this launcher but on other existing launchers as well.

If the launcher has to date not proved itself technologically, it has certainly done so scientifically. Properties of spherical deflagrations and detonations in $2H_2 + O_2$ mixtures diluted with H_2 or H_e at very high initial pressures, up to 1,000 psi, have been successfully studied. The transition limits from deflagration to detonation in the 8 in dia chamber for such mixtures have been determined. Deflagration and detonation velocities have been predicted and measured. Piezo-pressure gauges, heat-transfer gauges, ionization gauges, and photo diodes have been used as sensors to investigate such waves.

Lead azide, PETN, and cellulose nitrate have been successfully initiated at the surface by using gaseous detonation waves in planar and spherical geometries. This opens up a very interesting area of research which could not be pursued at UTIAS owing to the pressing problems of generating large projectile velocities and shock speeds. When this project was started we were advised by explosive experts that this could not be done. The successful initiation of shells of explosive made it possible to generate stable, focused, explosive-driven implosions in a safe, reuseable facility. This is a unique achievement and the possible technological applications may yet be numerous perhaps.

Gaseous implosion temperatures have been measured spectroscopically and it was shown that the maximum is indeed limited to about 5000°K. Their focusing properties have been determined by means of copper witness plates, image converter camera, and monitoring of total light output and at discrete wavelengths as a function of time using photomultiplier units. Projectile motion has been

20

studied using 34 Ghz (12 mm) microwaves and by employing 350 Kv X-ray units. The same type of measurements remain to be done with explosive-driven implosions.

The facility offers the possibilities of studying solids under extreme acceleration (10^{10} g's); material transformation from graphite to diamond at extreme pressures and temperatures, provided the impulse is of a sufficient size; production of dense plasmas (2 g/cc); high-energy sources for molecular beams; thermonuclear reactions (if the radiation losses are not prohibitive in reducing the temperature below 10^{7}°K, the densities are very attractive in the relation $n\tau = 10^{15}$, where n is particle/cc, τ in μsec); the study of elastic-plastic waves in cavities to provide design data for such chambers. (The latter was a particularly difficult problem in the design of the scaled-up version--24 in dia Launcher with a 1.0 in dia barrel for accelerating 13 g plastic projectiles to hypervelocities.)

The shock-tube operation makes use of 1.0 in dia diaphragm openings which are not so sensitive to off-focus implosions. Nor is it hampered by the difficulties of projectile integrity, erosion in small bores, or gas leakage problems around the projectile. In this mode we have already obtained shock velocities of 62,000 ft/sec using less than 100 g PETN explosive. It is in this area that the facility offers a great deal in the near future without apparent obstacles or excessive development. Consequently, this area of research is being pursued with a view of attaining flow velocities in the 100,000 ft/sec range, which should be uniform for at least 50 to 100 μsec in duration. Whether this goal will be achieved remains to be verified.

REFERENCES

1. Glass, I. I.   Shock and Combustion-Wave Dynamics in an Implosion-Driven Hypervelocity Launcher, UTIAS Review No. 25, January 1965.

2. Flagg,R. F.   The Application of Implosion Wave Dynamics to a Hypervelocity Launcher, UTIAS Report No. 125, June, 1967.

3. Dawson, V. C. D.   The MK II UTIAS Implosion-Driven Hypervelocity
   Waser,R. A.   Launcher Design Analysis, UTIAS Technical Note
   Oakes, D. O.   No. 147, March, 1970.

4. Czerwinski, W.   Structural Design and Development of UTIAS Implosion-Driven Launchers, UTIAS Report No. 153, (to be published).

5. Sevray, P.   Performance Analysis of UTIAS Implosion-Driven Launcher, UTIAS Technical Note No. 121, January 1968.

6. Flagg, R. F.   An Optimization Study of the UTIAS Implosion-Driven
   Mitchell, G. P.   Hypervelocity Launcher MKII, UTIAS Technical Note No. 130, December, 1968.

7. Garg, S. K.   Spherical Elastic-Plastic Waves in Solid Media, UTIAS Technical Note No. 132, February, 1969.

8. Benoit, A.   An Experimental Investigation of Spherical Combustion for the UTIA Implosion Driven Launcher, UTIAS Technical Note No. 71, September, 1963.

9. Benoit, A.   An Experimental Study of Spherical Combustion Waves
   Glass, I. I.   in a Hemispherical Chamber, Combustion & Flame, Vol. 12, No. 2, December, 1968, UTIAS Reprint No. 125.

10. Roberts, D. E.   A Spectroscopic Investigation of Combustion-Driven Spherical Implosion Waves, UTIAS Technical Note No. 140, August, 1969.

11. Makomaski, A. H.   Preliminary One-Dimensional Investigation of the Initiation of Low-Density PETN by Hydrogen-Oxygen Detonation Waves, UTIAS Technical Note No. 83, February, 1965.

12. Watson, J. D.   Implosion Driven Hypervelocity Launcher Performance Using Gaseous Detonation Waves, UTIAS Technical Note No. 113, May, 1967.

13. Poinssot, J. C.   A Preliminary Investigation of a UTIAS Implosion-
                              Driven Shock Tube, UTIAS Technical Note No. 136,
                              July, 1969.

14. Elsenaar, A.   Microwave Measurements of Projectile Motion in the
                              Barrel of the UTIAS Implosion Driven Hypervelocity
                              Launcher, UTIAS Technical Note No. 145,
                              September, 1969.

15. Chan, S. K.   Performance Trials of the Eight-Inch Diameter UTIAS
    Cappelli, G.   Implosion-Driven Hypervelocity Launchers MK II and
    Graf, W. O.   MK III, UTIAS Technical Note No. 161, (to be
                              published).

16. Kennedy, J. E.   Multipoint Initiated Implosions from Hemispherical
    Glass, I. I.   Shells of Sheet Explosive, UTIAS Technical Note
                              No. 99, December, 1966.

17. Glass, I. I.   Hypervelocity Launchers, Part 1: Simple Launchers,
                              UTIAS Review No. 22, January, 1963.

18. Glass, I. I.   Hypervelocity Launchers, Part 2: Compound Launchers·
                              Driving Techniques, UTIAS Review No. 26,
                              December, 1965.

19. Benoit, A.   Thermodynamic and Composition Data for Constant-
                              Volume Combustion of Stoichiometric Mixtures of
                              Hydrogen-Oxygen Diluted with Helium or Hydrogen,
                              UTIAS Technical Note No. 85, November, 1964.

20. Benoit, A.   Specific Heat Ratios and Isentropic Exponents for
                              Constant Volume Combustion of Stoichiometric Mixtures
                              of Hydrogen-Oxygen Diluted with Helium or Hydrogen,
                              UTIAS Technical Note No. 102, December, 1966.

21. Benoit, A.   Properties of Chapman-Jouguet Detonations in
                              Stoichiometric Hydrogen-Oxygen Mixtures Diluted
                              with Helium and Hydrogen, UTIAS Technical Note
                              No. 104, December, 1966.

22. Benoit, A.   Equilibrium Thermodynamic Data for the $H_2 - O_2 - He$
                              Systems, UTIAS Technical Note No. 128, August, 1968.

23. Elsenaar, A.   A Numerical Model for a Combustion-Driven Spherical
                              Implosion Wave, UTIAS Technical Note No. 144,
                              October, 1969.

24. Macpherson, A. K.   A Collisional Treatment of the Reflection of an
                              Imploding Hemispherical Shock Wave, Proceedings of
                              Seventh International Shock Tube Symposium, (to be
                              published).

25. Macpherson, A. K.   A Preliminary Study of Spherical Detonation Wave Symmetry in Stoichiometric Hydrogen Oxygen Mixtures, UTIAS Technical Note No. 154, (to be published).

26. Macpherson, A. K.   A Preliminary Monte-Carlo Analysis of the Reflection of an Imploding Hemispherical Shock Wave Similar to that Generated in the UTIAS Implosion Driven Hypervelocity Launcher of Shock Tube, UTIAS Report No. 152, (to be published).

27. Glass, I. I.   Implosion-Driven Shock Tube, Proceedings of Seventh
    Poinssot, J. C.   International Shock Tube Symposium, (to be published).

28. Benoit, A.   Thermodynamic Properties for Gaseous Mixtures Used in Hypervelocity Techniques. Revue Engrgie Primaire, Vol. IV, No. 4, 1968, UTIAS Reprint No. 127.

29. Flagg, R. F.   Explosive-Driven Spherical Implosion Waves, The
    Glass, I. I.   Physics of Fluids, Vol. 11, No. 10, October, 1968. UTIAS Reprint No. 122.

30. Garg, S. K.   Numerical Solutions for Spherical Elastic-Plastic Wave Propagation, Journal of Applied Mathematics & Physics (Zamp) Vol. 19, Fasc. 5, 1968, pp. 778-787, UTIAS Reprint No. 119.

31. Garg, S. K.   Spherical Elastic-Plastic Waves, Journal of Applied Mathematics & Physics (Zamp) Vol. 19, Fasc. 2 (1968) pp. 243-251, UTIAS Reprint No. 116.

32. Flagg, R. F.   Ionization Gauge Circuit for Detection of Multiple Shock and Reflected Detonation Waves, The Review of Scientific Instruments, Vol. 38, No. 9, pp. 1336-1337, September 1967, UTIAS Reprint No. 106.

33. Glass, I. I.   Research Frontiers at Hypervelocities, Canadian Aeronautics and Space Journal, Vol. 13, No's 8 & 9, pp. 348-366, 401-426, October and November 1967, JTIAS Reprint No. 114.

34. Crowley, B. K.   Numerical Simulation of a High-Energy (Mach 120 to
    Glenn, H. D.   40) Air-Shock Experiment, Proceedings of Seventh International Shock Tube Symposium, (to be published).

35. Brode, H. L.   Theoretical Description of the Performance of the UTIAS Hypervelocity Launcher, Second International Colloquium on Gasdynamics of Explosions and Reactive Systems, Akademgorodok, Novosibirsk, Aug. 24-29, 1969, Proceedings, Astronautica Acta (to be published).

36. Brode, H. L.   Numerical Solutions of Spherical Blast Waves, Jl. Appl. Phys. 26, 6, p. 766, 1955.

37. Brode, H. L.   Numerical Calculations of Blast Waves, Rand Corp., Rept. P-1933, 1960. (The initial computations for the UTIAS Launcher were performed by Dr. H. L. Brode--private communications, 1962.)

38. Brode, H. L.   Blast Wave from a Spherical Charge, Phys. Fluids, 2, 2, p. 217, 1959.

39. Graf, W. O.   A Study of Projectile Integrity under Extreme Conditions in an Implosion-Driven Hypervelocity Launcher, University of Toronto Ph.D. Thesis (in progress).

40. Chan, S. K.   A Theoretical and Experimental Study of Implosion-Driven Shock Tubes, University of Toronto Ph.D. Thesis (in progress).

41. Lee, J. H.   Theory of Explosions, MERL Report 69-10,
    Knystautus, R.   McGill University, Dept. of Mechanical Eng.
    Bach, G. G.   Montreal, 1969.

42. Huni, J. P. R.   A Study of Concentric Imploding Detonations, University of British Columbia, Ph.D. Thesis, 1970.

43. Seigel, A. E.   Theory of High Speed Guns, Agardograph 91, 1965.

44. Lukasiewicz, J.   Constant Acceleration Flows and Application to High-Speed Guns, AEDC TR-66-181, 1966.

45. Watson, J. D.   High-Velocity Explosively Driven Guns, Physics International NASA CR-1533, 1970.

46. Titov, V. M.   Acceleration of Solid Bodies by Cumulative
    Fadeenko, Yu. I.   Explosions, Second International Colloquium on Gasdynamics of Explosions and Reactive Systems, Akademgorodok, Novosibirsk, Aug. 24-29, 1969, Proceedings, Astronautica Acta (to be published).

47. Boyer, A. G.   Design, Instrumentation and Performance of the UTIAS 4 in x 7 in Hypersonic Shock Tube, UTIAS Report No. 99, 1964.

48. Warren, W. R.   A Critique of High Performance Shock Tube Driving
    Harris, C. J.   Techniques, Proceedings, Seventh International Shock Tube Symposium, Edited by I. I. Glass, University of Toronto Press, 1970.

Note added in proof: Ref. 35 is now available as a Rand Corp. Report RM-6298-PR, July, 1970.

26
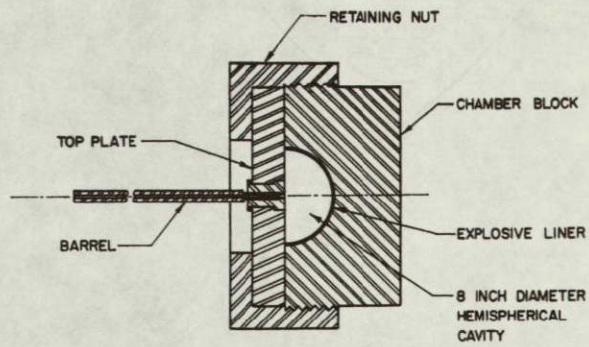
Figure 1
Schematic view of the UTIAS implosion-driven hypervelocity launcher

Labels: RETAINING NUT, CHAMBER BLOCK, TOP PLATE, EXPLOSIVE LINER, BARREL, 8 INCH DIAMETER HEMISPHERICAL CAVITY
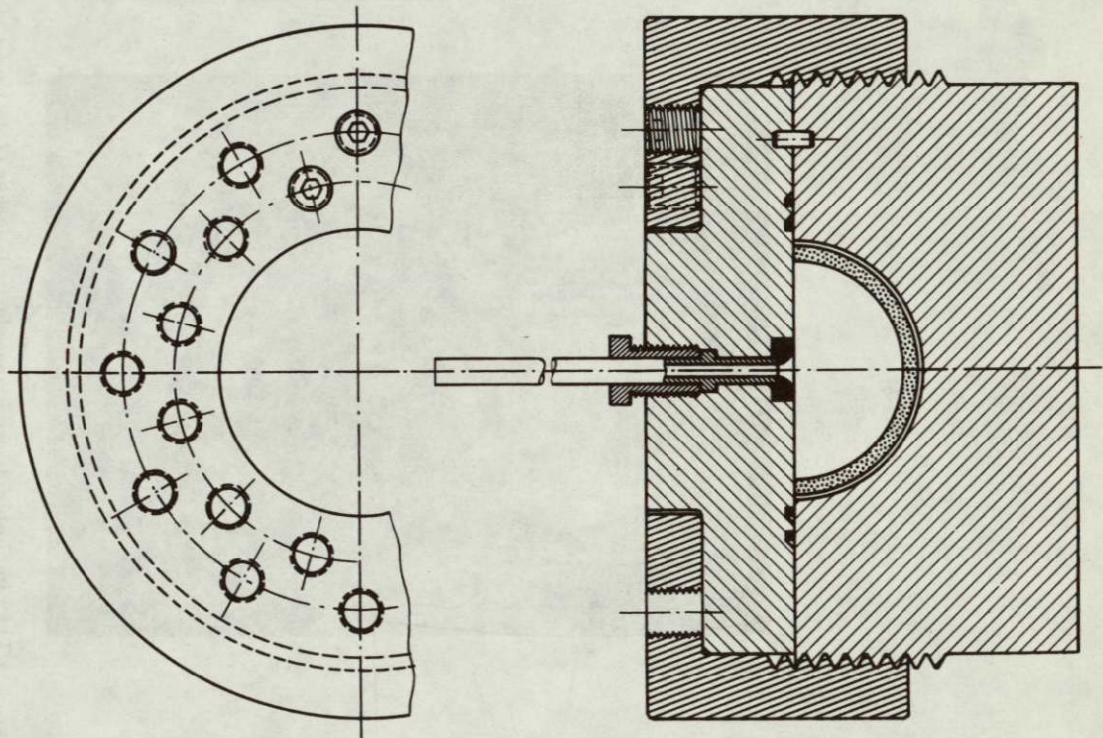
Figure 2

UTIAS IMPLOSION-DRIVEN HYPERVELOCITY LAUNCHER, MARK I,
CAVITY 8 in dia, BARREL 0.22 in dia or 0.313 in dia x 4 to 6 ft long
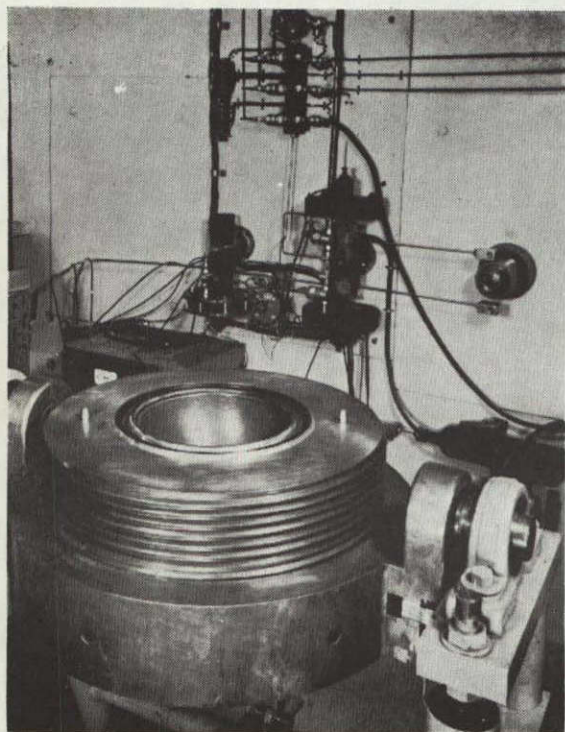
Figure 3
View of the hemispherical chamber in the opened position
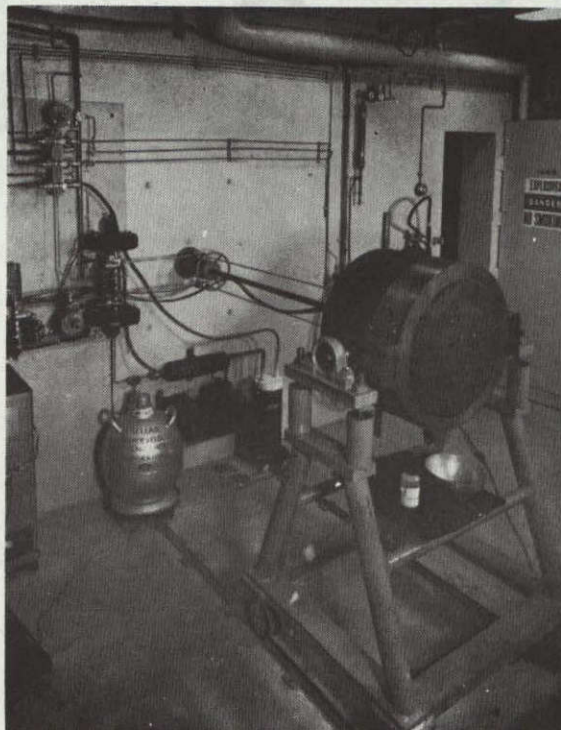
Figure 4
UTIAS implosion-driven hypervelocity launcher (Gun barrel
0.22 calibre, retaining nut, chamber block, 8 in. dia. ×
1/10 in. thick metal liner shell, a bottle of explosive, and a
0.22 in. dia. × 1 calibre long polyethylene projectile
are shown.)
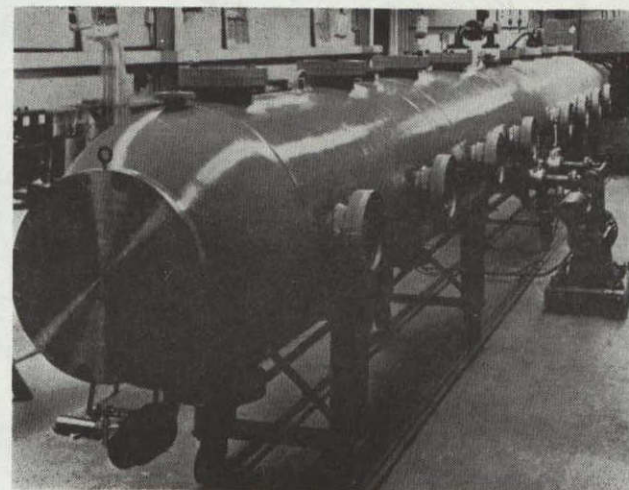
Figure 5
View of the ballistics range

BARREL — PROJECTILE
EXPLOSIVE LINER
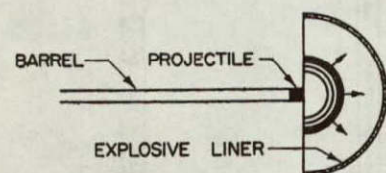
(a) Ignition phase: A gaseous detonation wave propagates outward from the origin in a $2H_2 + O_2$ mixture
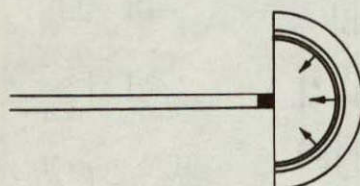
(b) Implosion phase: The detonation wave initiates the explosive liner, which in turn generates a strong imploding wave
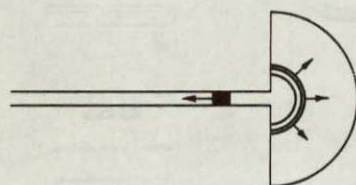
(c) Reflection phase: The implosion wave reflects from the origin leaving a region of high-pressure, high-temperature gas which bursts the diaphragm behind the projectile accelerating it to hypervelocity

Figure 6
Schematic diagram illustrating the principle of operation of the implosion-driven hypervelocity launcher
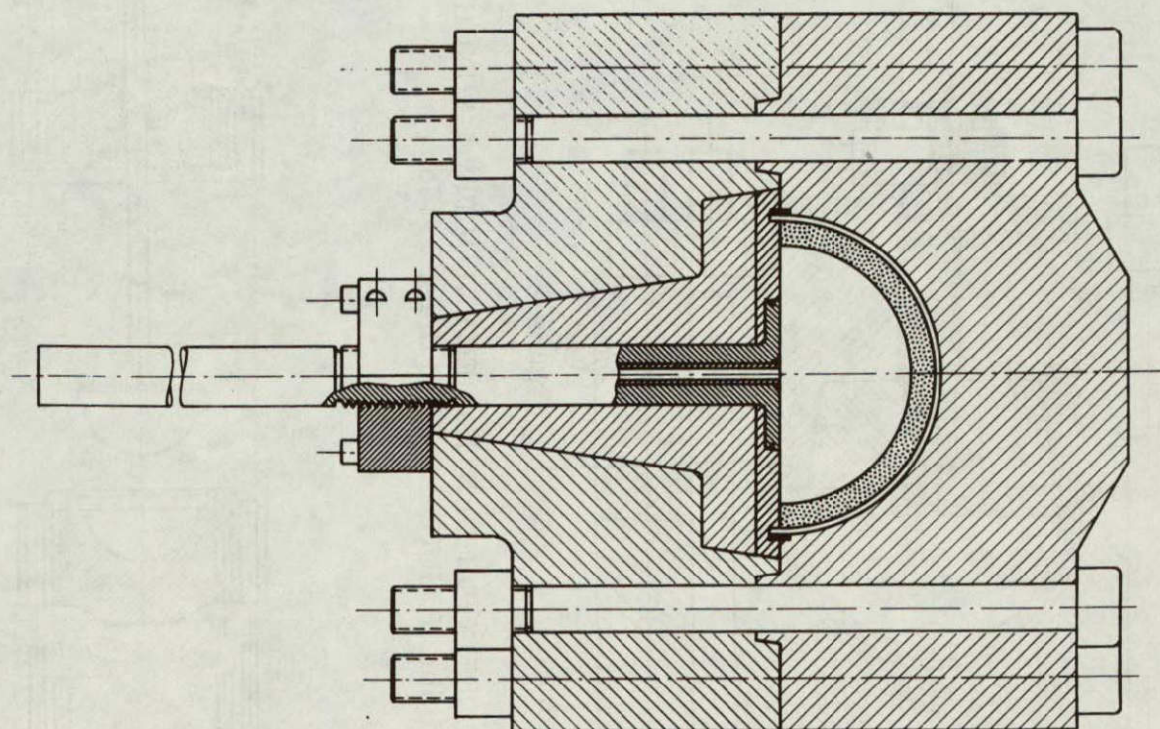
Figure 7

UTIAS IMPLOSION-DRIVEN HYPERVELOCITY LAUNCHER, MARK II, CAVITY 8 in dia, BARREL 0.22 in dia x 2 ft long

29
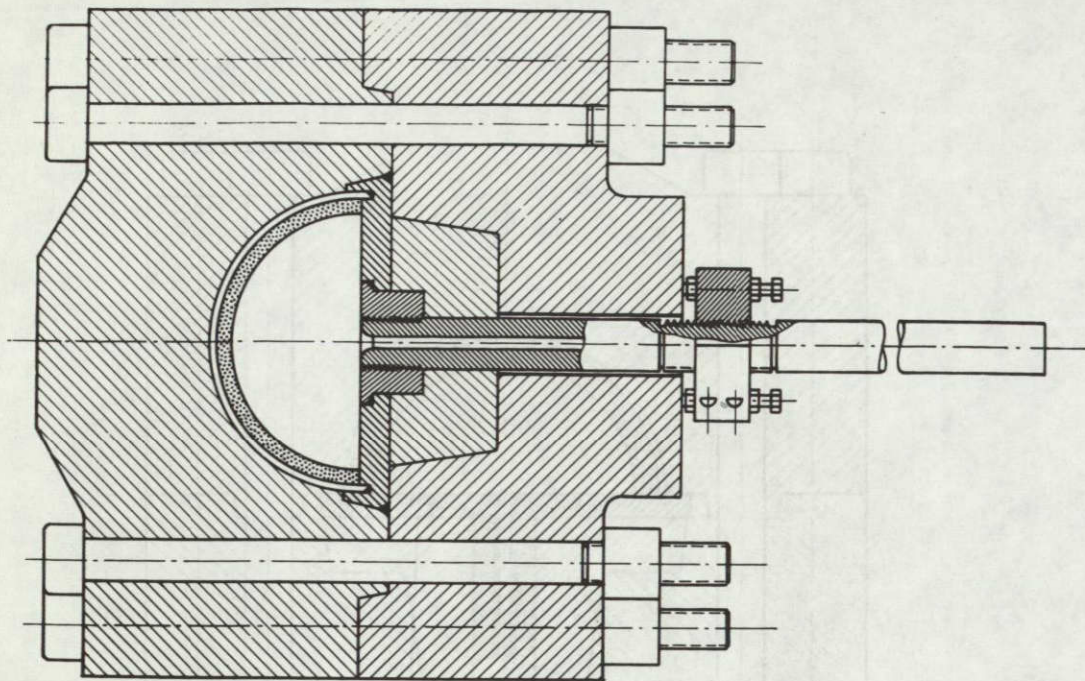
Figure 8

UTIAS IMPLOSION-DRIVEN HYPERVELOCITY LAUNCHER, MARK III,
CAVITY 8 in dia, BARREL 0.22 in dia x 2 ft long
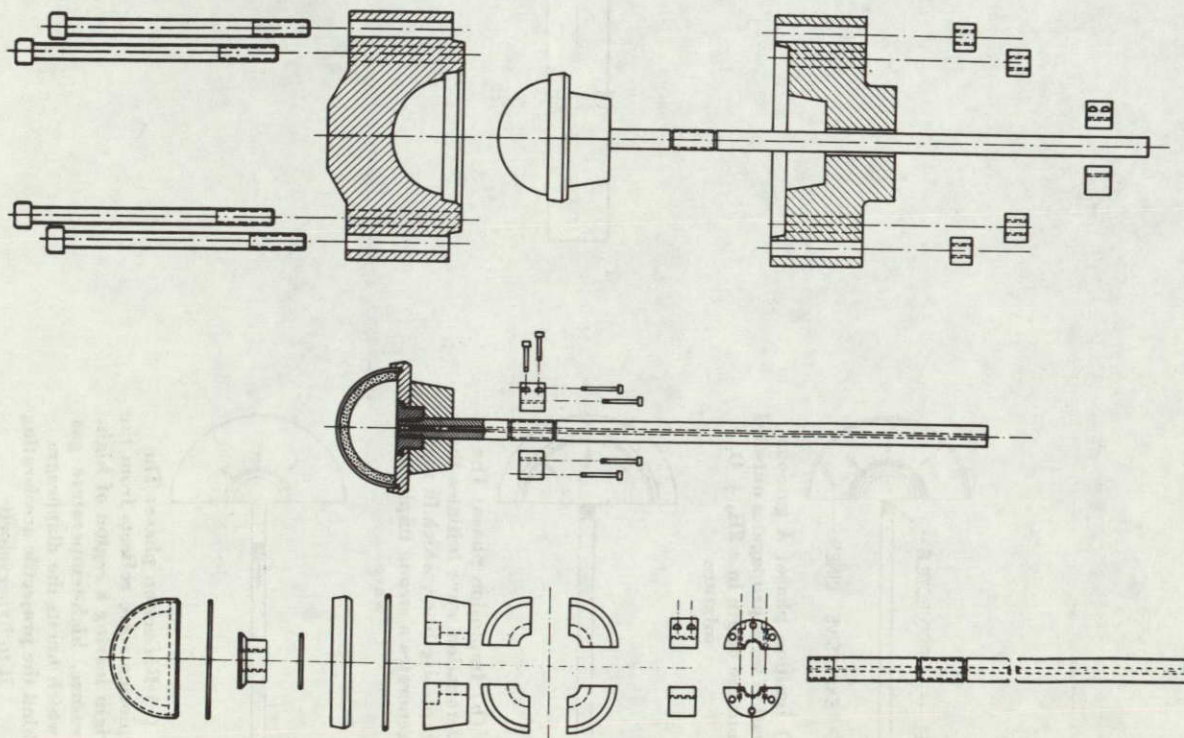
Figure 9

UTIAS IMPLOSION-DRIVEN HYPERVELOCITY LAUNCHER, MARK III,
EXPLODED VIEW, 8 in dia or 24 in dia CAVITY, 0.22 in dia or 1.0
in dia BARREL

UTIAS IMPLOSION-DRIVEN HYPERVELOCITY LAUNCHER

DATA: 1) 24 IN DIA HEMISPHERICAL IMPLOSION CHAMBER

2) I IN DIA X 13 FT LONG BARREL

3) OVERALL WEIGHT 32,600 LB.
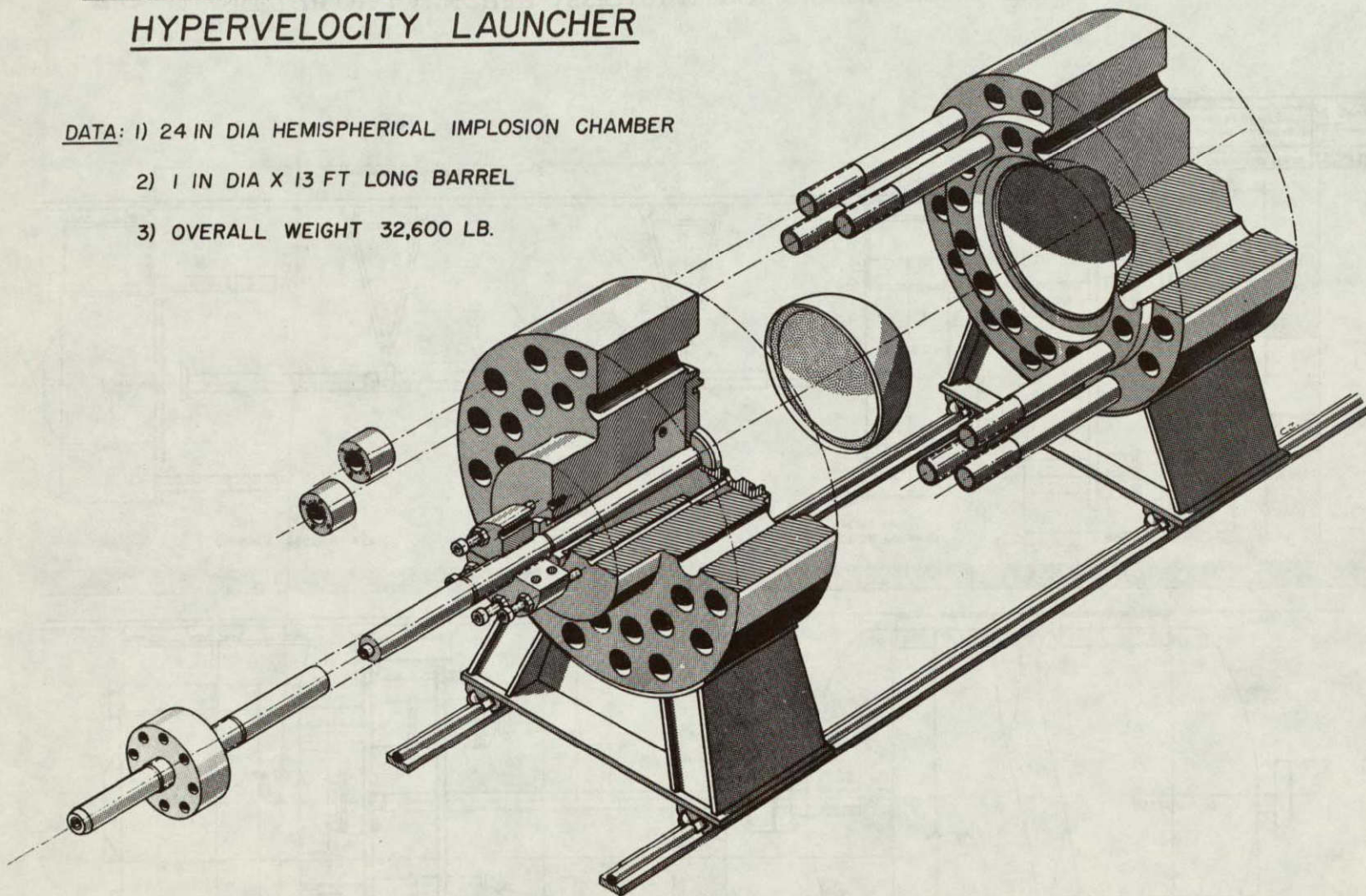
FIG. 10   PERSPECTIVE VIEW OF 24 IN. DIA. MK II UTIAS IMPLOSION-DRIVEN HYPERVELOCITY
LAUNCHER
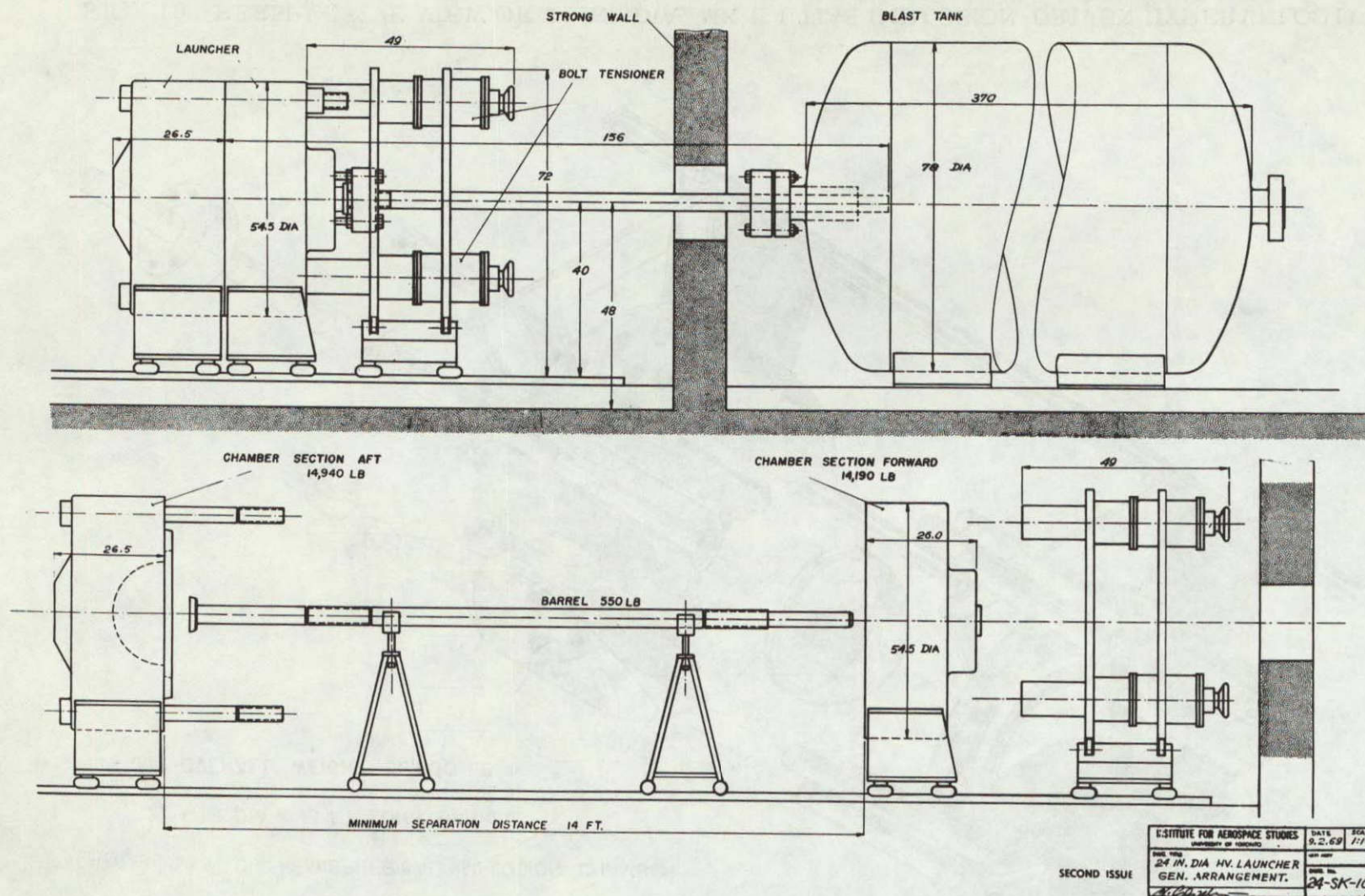
FIG. 11   SKETCH OF LAUNCHER ASSEMBLY SHOWING THE BOLT-TENSIONER MECHANISM
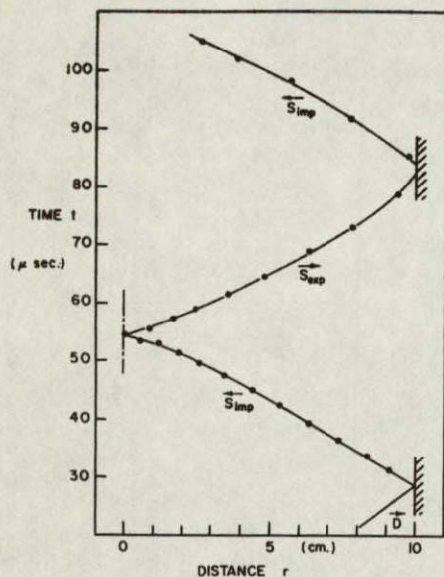
Figure 12
Wave trajectories for 100 psia of a mixture of
$2H_2 + O_2 + 7He$ ($\gamma = 1.67$) in an 8 in. dia. hemisphere
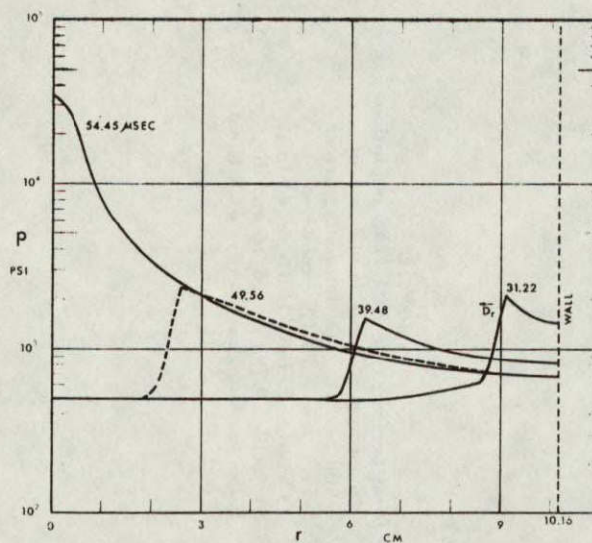
Figure 13 (a)
Conditions in an 8 in. dia. hemispherical hypervelocity
launcher chamber following the detonation of a combustible
gas mixture ($2H_2 + O_2 + 7He$). Variation of pressure with
radius as a function of time. $p_1 = 100$ psi, $T_1 = 290°K$,
$\rho_1 = 1.82 \times 10^{-3}$ gm/cm³, D_r = reflected detonation wave
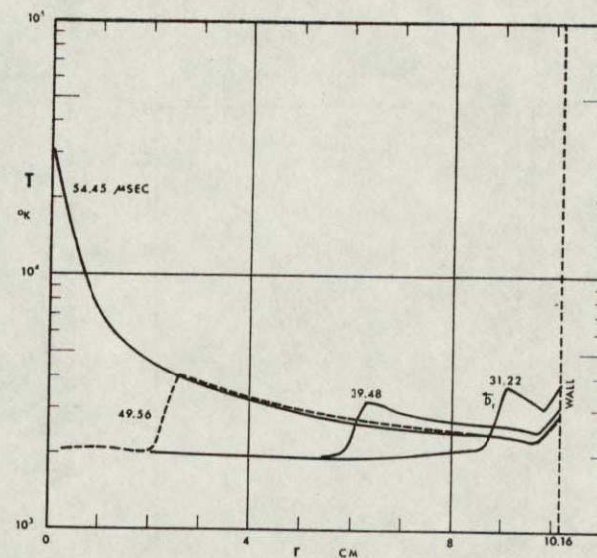
Figure 13 (b)
Conditions in an 8 in. dia. hemispherical hypervelocity
launcher chamber following the detonation of a combustible
gas mixture ($2H_2 + O_2 + 7He$). Variation of temperature
with radius as a function of time . $p_1 = 100$ psi,
$T_1 = 290°K$, $\rho_1 = 1.82 \times 10^{-3}$ gm/cm³, D_r = reflected
detonation wave
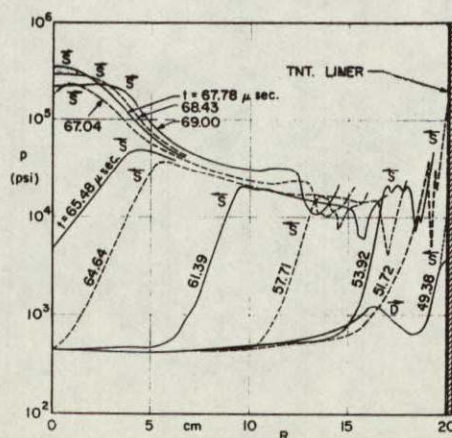
Figure 14
Conditions in a 16 in. dia. hemispherical hypervelocity
launcher chamber following the detonation of a combustible
gas mixture ($2H_2 + O_2 + 7He$) and a 0.1 in. thick
hemispherical liner of TNT. Variation of pressure with
radius as a function of time.
$p_1 = 100$ psi, $T_1 = 290°K$, $\rho_1 = 1.82 \times 10^{-3}$ gm/cm³,
D = detonation wave, S = shock wave
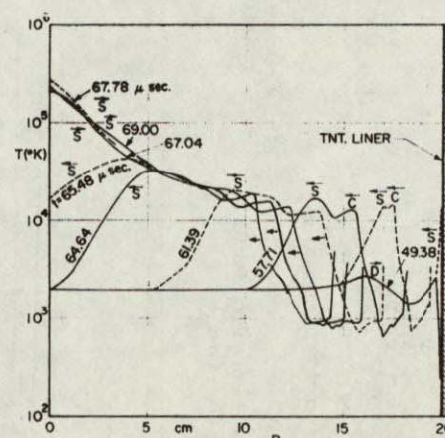
Figure 15
Conditions in a 16 in. dia. hemispherical hypervelocity
launcher chamber following the detonation of a combustible
gas mixture ($2H_2 + O_2 + 7He$) and a 0.1 in. thick
hemispherical liner of TNT. Variation of temperature with
radius as a function of time.
$p_1 = 100$ psi, $T_1 = 290°K$, $\rho_1 = 1.82 \times 10^{-3}$ gm/cm³,
D = detonation wave, S = shock wave, C = contact front
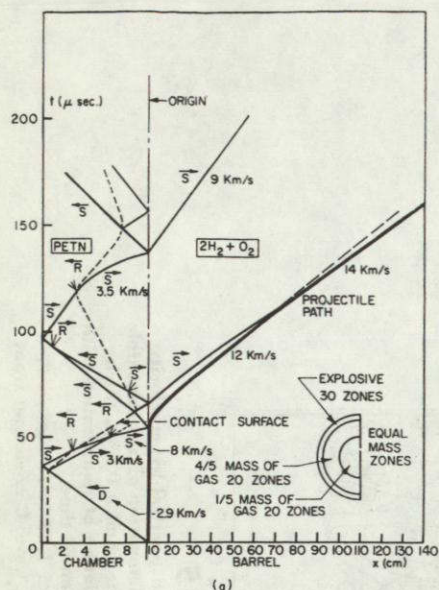
(a) Ideal (x, t) plane wave diagram for 200 gm PETN—Case 1
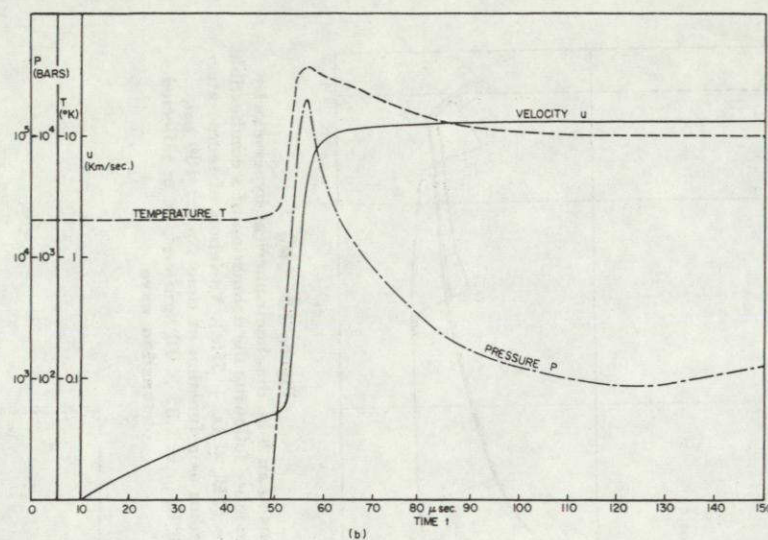
(b) Pressure and temperature at the base of the projectile and projectile velocity as function of time (for barrel length, see (a))

Figure 16

Ideal performance of UTIAS implosion-driven hypervelocity launcher using a 200 psi $2H_2 + O_2$ detonating driver gas + PETN explosive. Chamber radius: 10.16 cm (4 in.), projectile: 0.793 cm (5/16 in.) dia. $\times$ 0.793 cm long, gas energy: 44.8 K cal.
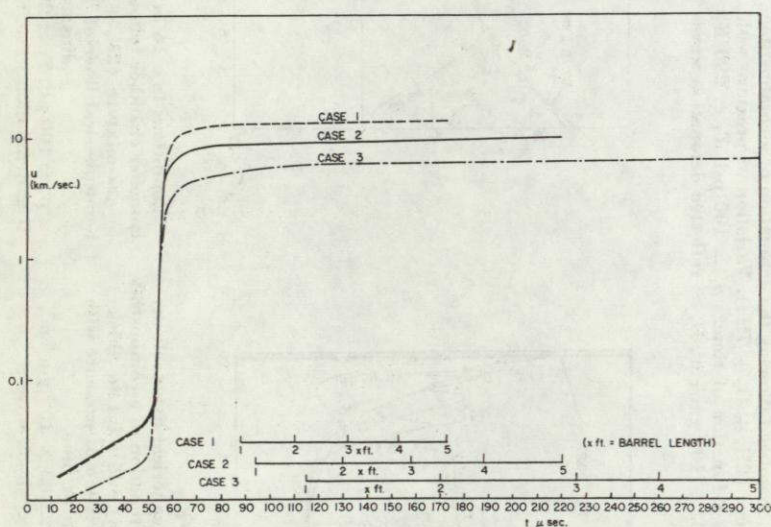
(c) Projectile velocities as a function of time and barrel length for the three cases noted below

	Case 1	Case 2	Case 3
Weight of $2H_2 + O_2$ gas –gm	12	14	14
PETN weight –gm	200	100	100
Projectile weight –mg	356 polyethylene	356 polyethylene	712 magnesium
$mass_{barrel\ gas}/mass_{proj}$	6.8	2.1	0.9
E_{exp}/E_{gas}	7	2.8	2.8
E_{proj}/E_{total}	0.030	0.027	0.022
Peak acceleration –g's	$1.4 \times 10^3 P_{max}$	$1.4 \times 10^3 P_{max}$	$0.7 \times 10^3 P_{max}$
Muzzle velocity at 5 ft.—km/sec.	13.6	9.9	6.7
Actual velocities — km/sec.	projectile shattered	5 distorted (86 gm PETN)	3 survived (76 gm PETN)

Notes.
1. Without explosive there are 15.5 gm of driver gas at 200 psi; the amount decreases with explosive thickness.
2. The ratios of outflow into the barrel of driver gas to projectile mass[50] are compared for the three runs and the non-linear nature of the problem is illustrated. The higher the projectile velocity the more driver gas is required. The outflow is subsonic in all cases due to the persisting high temperatures.[77]
3. The effects of total energy or explosive-to-gas energy ratio and that of projectile mass can also be seen in the table.
4. The chemical to projectile kinetic energy conversion for all cases is low (2 to 3%) and is best at the highest velocities.
5. About half the predicted velocity was obtained where the projectile did not shatter (see Table 3).

34
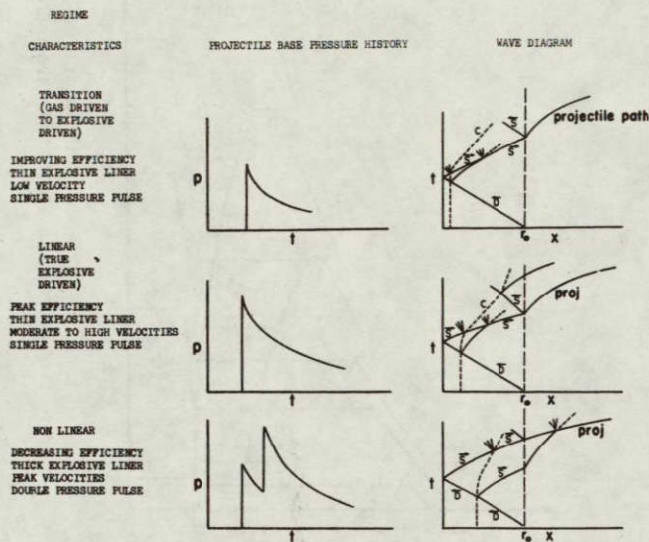
Figure 17 SCHEMATIC DIAGRAM OF THE OPERATING REGIMES OF AN IMPLOSION DRIVEN
HYPERVELOCITY LAUNCHER (SEE ALSO REF. 4)

Figure 18 MUZZLE VELOCITY AS A FUNCTION OF INITIAL PRESSURE
AND EXPLOSIVE LOADING FOR A SINGLE-CALIBRE PROJEC-
TILE, 5/16 in. dia., 356 mg (1g/cc), FOR A 5 ft. BARREL

Figure 19 OPTIMUM CASE IN THE 8 in. dia. CHAMBER

Pressure and temperature at the base of one-caliber
(0.22 in) projectile, and projectile velocity versus
distance.

400 g PETN
Initial Gas pressure: 200 psi , $2H_2 + O_2$

Figure 20

OPTIMUM CASE FOR THE 30 in. dia. CHAMBER
Pressure and temperature at the base of one-caliber, 1 in. dia.
projectile, and projectile velocity versus time.

18.5 Kg PETN
Initial Gas pressure: 200 psi , $2H_2 + O_2$

Figure 21
PRESSURE AT THE EXPLOSIVE-METAL INTERFACE
AS A FUNCTION OF TIME FOR THE DESIGN CASE

PRESSURE AT EXPLOSIVE-METAL INTERFACE (bars)

TIME (microseconds)

Figure 22
TOTAL FORCE ON THE BREECH BLOCK
VS TIME FROM INITIATION

REFLECTION FROM CONTACT SURFACE

EXPLOSIVE COMPLETELY DETONATED

REFLECTION FROM OUTER WALL

INSTANT OF IMPLOSION

PROJECTILE EXITS BARREL

MIN & MAX TO t=4600 μsec

EXPLOSIVE INITIATES

MINIMUM LOAD AT 200 PSIA

30"DIA CHAMBER
200 PSIA 2H₂ + O₂
25 KG PETN @ 0.5886/CC

TOTAL FORCE ON BREECH BLOCK (pounds)

TIME (microseconds)

CAVITY SURFACE DISPLACEMENT ū₀(in)

GARG
GRAF

TIME t̄(μsec)

Figure 23 CAVITY SURFACE DISPLACEMENT

PARTICLE VELOCITY (V x10²)

0.2
0.3
0.5
0.7
2.0
t=0.05
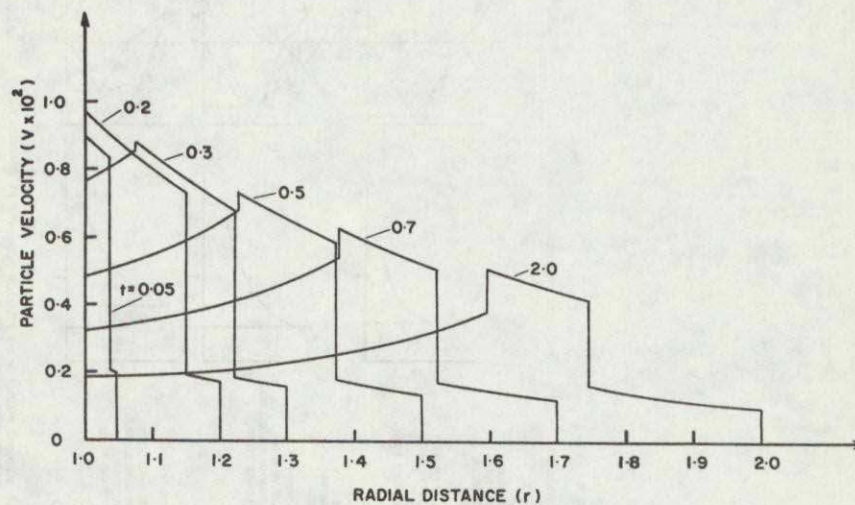
RADIAL DISTANCE (r)

Figure 24 PLOT OF PARTICLE VELOCITY VERSUS RADIAL DISTANCE

IMPLOSION-DRIVEN SHOCK TUBE

(x,t) – DIAGRAM

Figure 25. WAVE-SPEED DIAGRAM IN THE (x,t) PLANE FOR A UTIAS IMPLOSION-DRIVEN SHOCK TUBE

$2H_2 + O_2$

$M_s = 95$

200 PSI (13.6 ATM.) $2H_2 + O_2$
200 g PETN
I TORR COUNTERPRESSURE
8 IN (20 CM) DIA CHAMBER
5/16 IN (8 MM) DIA BARREL

AIR

Figure 26. SHOCK TUBE CASE PRESSURE PROFILES

200 PSI (13.6 ATM) $2H_2 + O_2$
200 g PETN
I TORR COUNTERPRESSURE, AIR
8 IN (20 CM) DIA CHAMBER
5/16 (8MM) DIA BARREL

—— t = 107.65 μs
– – – t = 206.50 μs
········ t = 306.92 μs
–·–·– t = 407.36 μs
• INTERFACE

37

FIGURE **27** Geometrical configuration and positions of observation stations
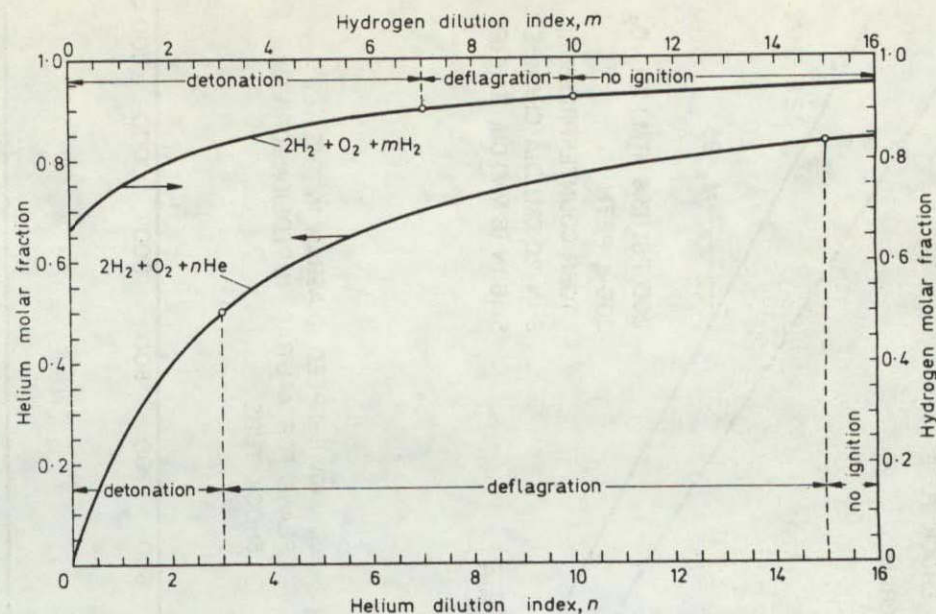
FIGURE **28** Deflagration and detonation limits associated with the present ignition system
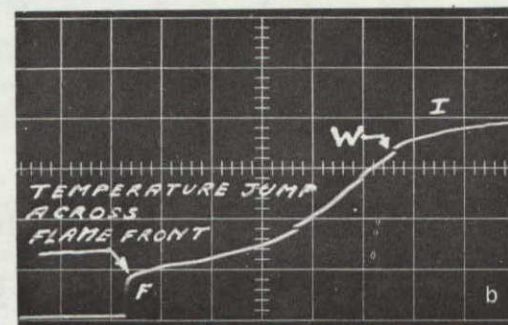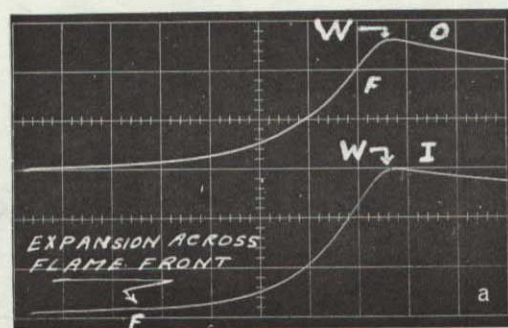
FIGURE **29** Deflagration heat transfer and pressure histories: (a) Pressure records. Vertical scales: I 219 (lb/in^2)/div., O 236 (lb/in^2)/div.; horizontal scale 1 msec/div. (b) Heat transfer record (I). $R_0 = 26\,\Omega$; $i = 20$ mA. Vertical scale: 20 mV/div.; horizontal scale: 1 msec/div. Initial conditions: mixture $2H_2 + O_2 + 7He$; pressure 100 lb/in^2; temperature 297°K
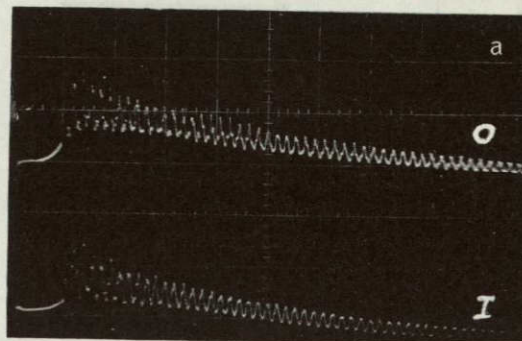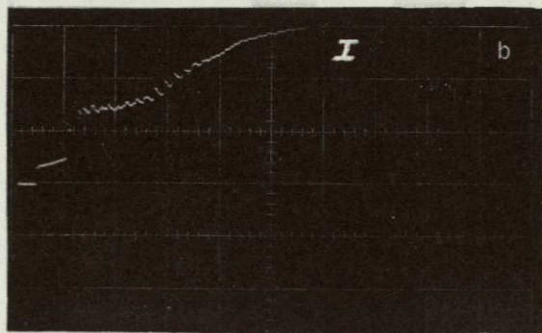
FIGURE **30** Heat transfer and pressure histories in detonating combustion. Initial mixture: $2H_2 + O_2 + 2He$. Initial pressure 100 lb/in². Initial temperature 294°K. Time scales 1 msec/div. (a) Pressure histories: I: 697 (lb/in²/div.; O: 876 (lb/in²)/div. (b) Heat transfer histories (I). $R_0 = 250\,\Omega$; $i = 25$ mA; 1 V/div.
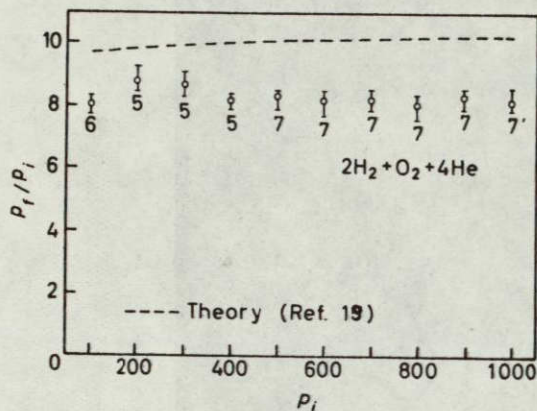
FIGURE **31** Final-to-initial pressure ratio after complete combustion (p_f/p_i) versus initial pressure (p_i)
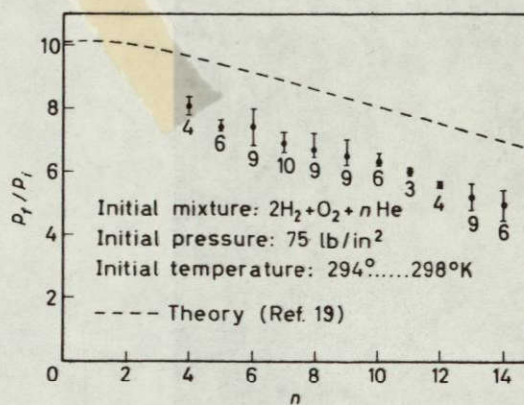
FIGURE **32** Final-to-initial pressure ratio after complete combustion (p_f/p_i) versus dilution n
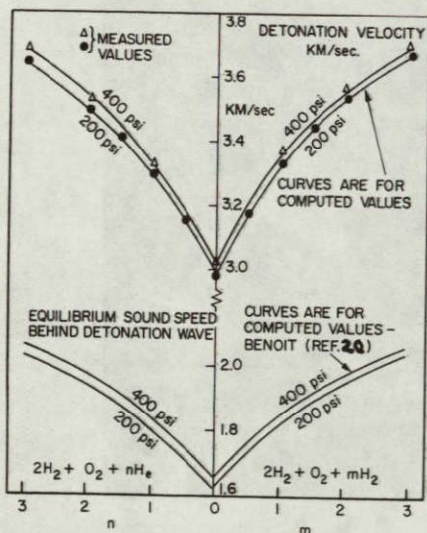
(b) Detonation velocities as functions of initial pressure and helium or hydrogen dilution
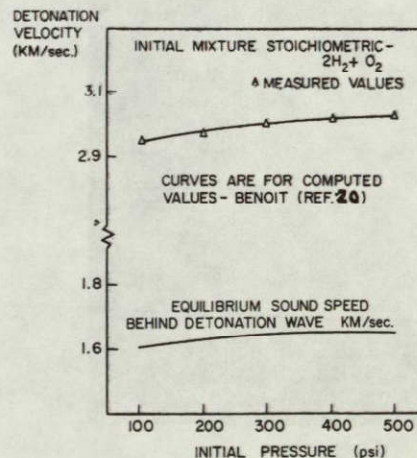
(a) Detonation velocities for stoichiometric mixtures as a function of initial pressure

Figure **33**
Detonation velocities in hydrogen-oxygen mixtures

(a)   (b)
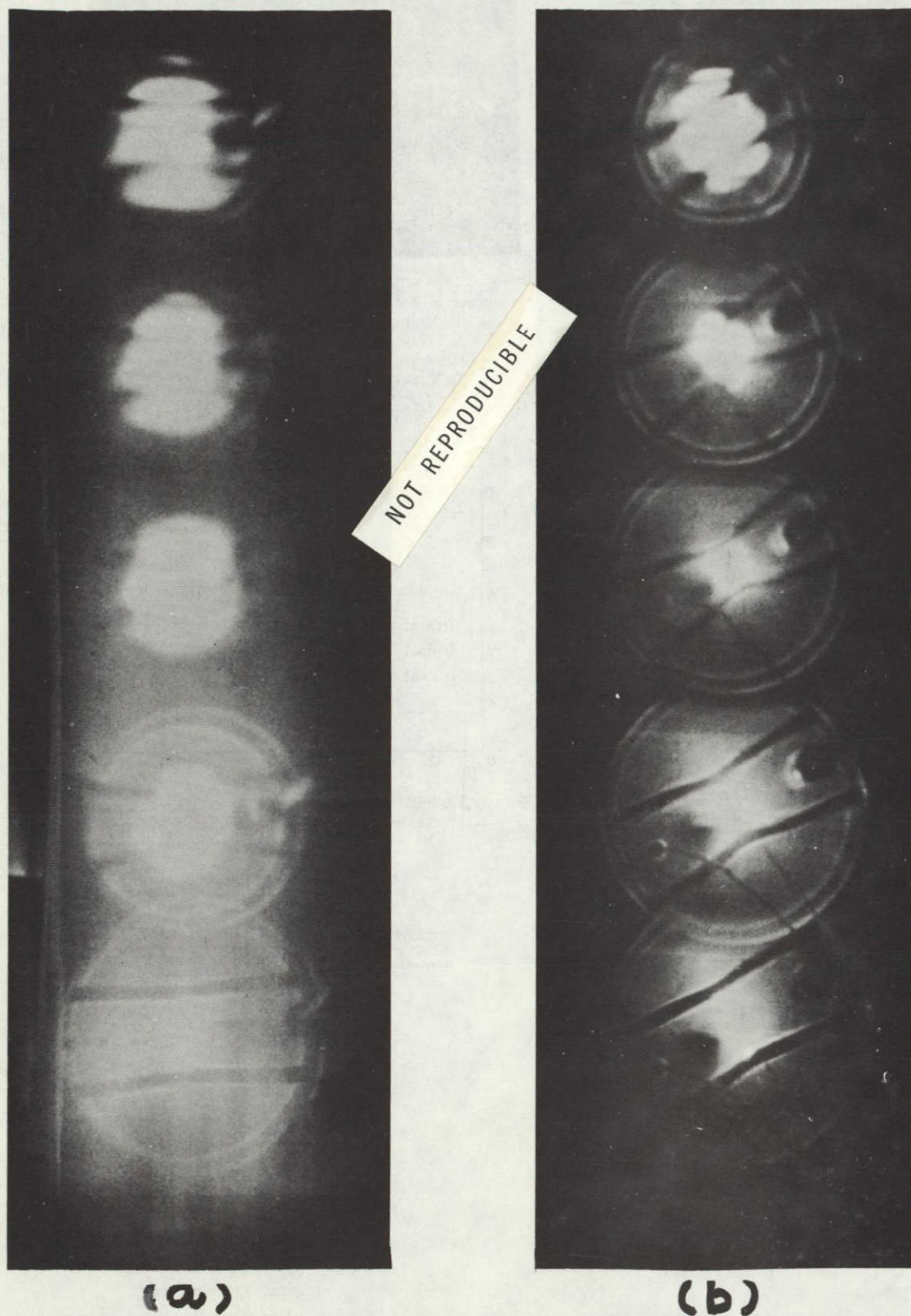
FIG   34   FRAMING CAMERA PICTURES OF DETONATION INITIATED
              BY AN EXPLODING WIRE

     a) 200 psia initial $2H_2+O_2$ mixture; times after
         initiation in μ sec, 0.1, 20.1, 40.1, 60.1, 80.1.

     b) 400 psia initial $2H_2+O_2$ mixture; times after
         initiation in μ sec, 0.1, 5.1, 10.1, 15.1, 25.1.

IONIZATION PROBE LOCATIONS

IGNITION CABLE CONNECTOR

EXPLODING WIRE

WITNESS CUP

EXPLOSIVE

0 5 10
cm.
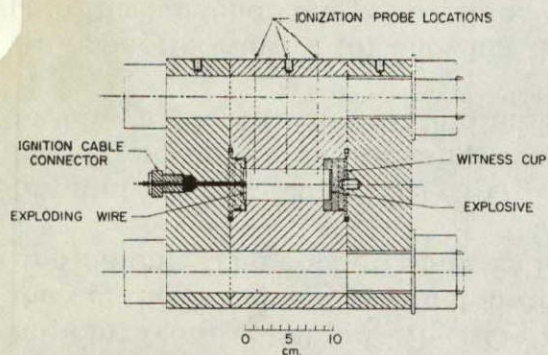
Figure 35
Cross-section of one-dimensional chamber
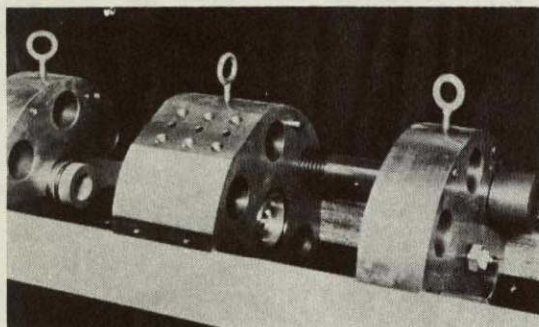
(a) Container for holding explosives (extreme left)
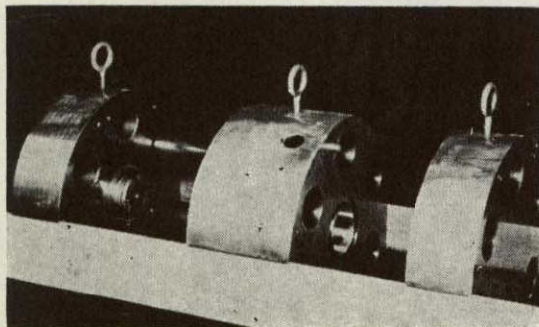
(b) Opposite view of electrode and ignition wires (also at extreme left)

Figure 36
One-dimensional combustion chamber

TIME FROM REFLECTION t (μ sec.)

SLOPE⁻¹ = 1.79 KM/sec.

SYMBOL	RUN NUMBER	INITIAL PRESSURE
□	42	270 psia
△	40	180 psia
○	32	90 psia

DISTANCE x
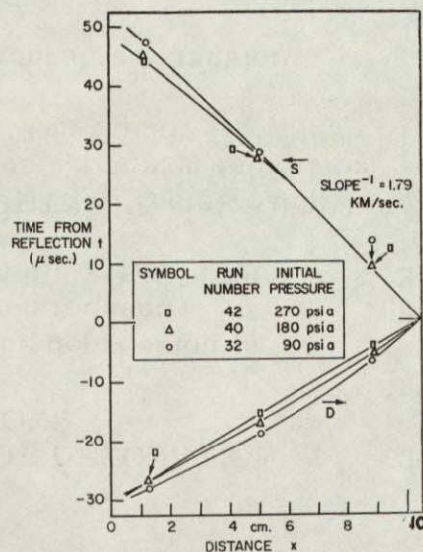
Figure 37
Wave front diagrams for $2H_2 + O_2$ in the one-dimensional chamber for several values of initial pressure

TIME FROM REFLECTION t (μ sec.)

REFLECTED SHOCK TRAJECTORY FOR NO EXPLOSIVE

SYMBOL	RUN NUMBER	INITIAL PRESSURE	E_0/P
△	170	30 psia	48.8
□	67	89 psia	9.17
○	58	92 psia	4.60

DISTANCE x
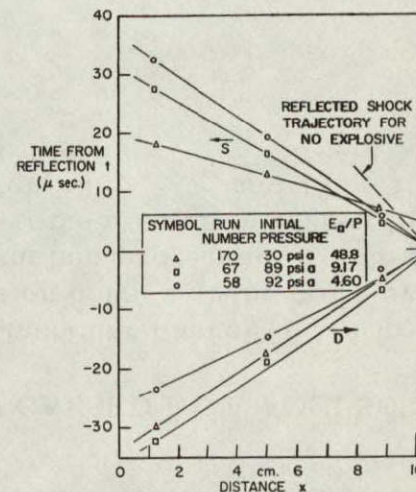
Figure 38
Wave front diagrams for lead azide in the one-dimensional chamber for several values of initial pressure

W = 4.229 gm.
DENSITY = 1.0 gm/cc.

REFLECTED SHOCK TRAJECTORY FOR NO EXPLOSIVE

TIME FROM REFLECTION t (μ sec.)

SYMBOL	RUN NO.	INITIAL PRESSURE	E_0/P_1
□	18	160 psia	47.2
○	43	180 psia	42.0
△	38	270 psia	24.0

DISTANCE x
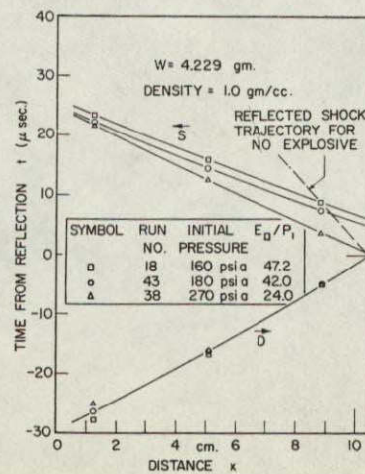
Figure 39
Wave front diagrams for PETN pressings in the one-dimensional chamber for several values of initial pressure

TIME FROM REFLECTION t (μ sec.)

DEFLAGRATION

DETONATION

SYMBOL	RUN NO.	INITIAL PRESSURE	E_0/P_1
○	194	25.1 psia	
□	199	50.0 psia	49.5
△	202	100.0 psia	37.4

DISTANCE x
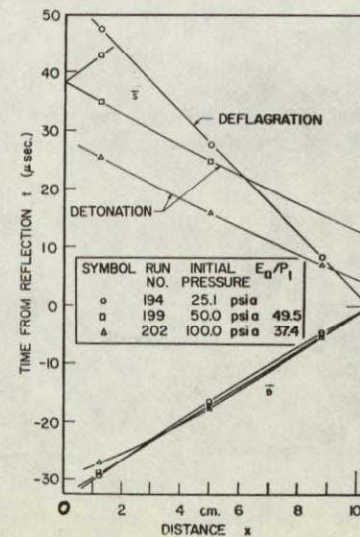
Figure 40
Wave front diagrams for Superfine PETN in the one-dimensional chamber for several values of initial pressure
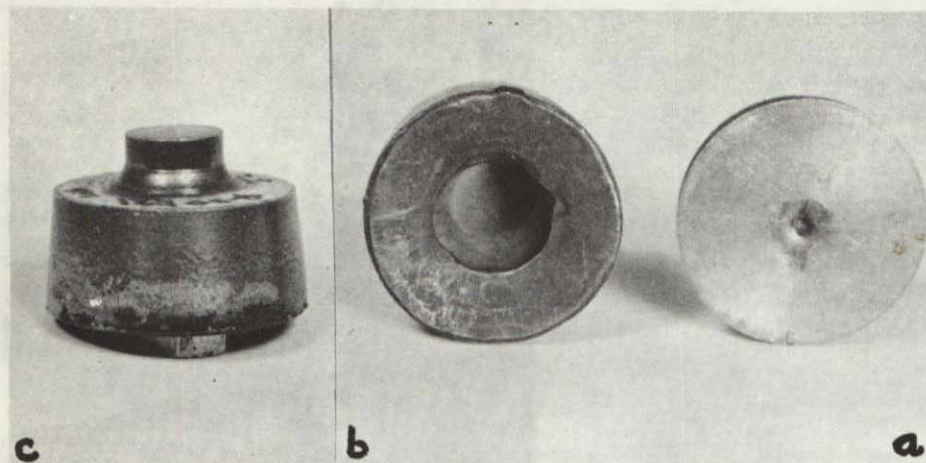
Figure 41

Figure 42

IMPRINTS IN COPPER WITNESS-PLATES OF DETONATION
AND EXPLOSIVE-DRIVEN IMPLOSIONS

a) Imprint from a 400 psi $2H_2 + O_2$ run.   The depression in
the centre is caused by a detonation-driven focused
implosion.   The copper plate is 1 5/16 in dia x 1/4 in thick.

b) Imprint from a 400 psi $2H_2 + O_2$ + 88 g PETN.   The sizeable
crater caused by the focusing of the explosive driven implosion
is very evident (same plate diameter x 1/2 in thick).

c) An opposite view of (b) showing the considerable extrusion
into the launcher barrel orifice.
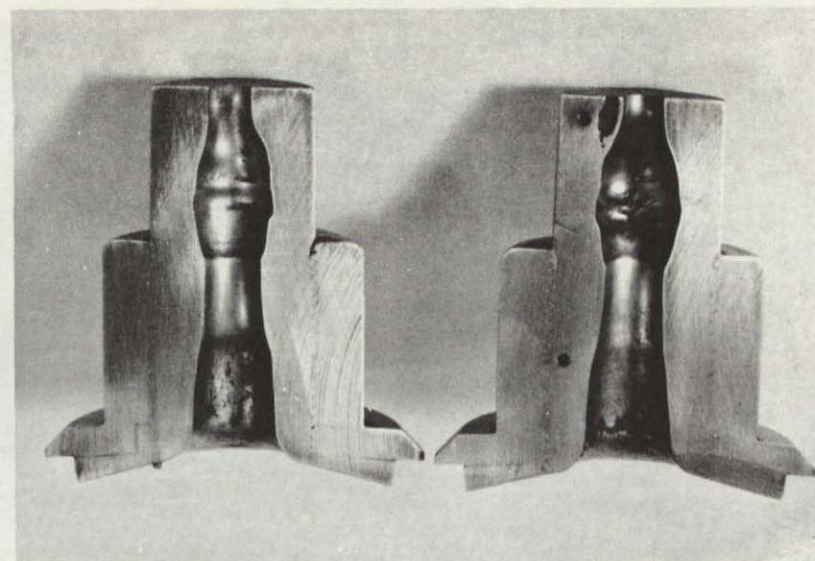
THE EROSION CAUSED BY A FOCUSED IMPLOSION

The sectioned launcher barrel (1 1/4 in od x 0.213 id)
shows the erosion caused at the point even where the
half-calibre titanium projectile (0.253 g) was located
2.0 in from the origin so as to lessen the effects of the
implosion (400 psi $2H_2 + O_2$ and 125 g PETN; projectile
velocity 11,000 fps)
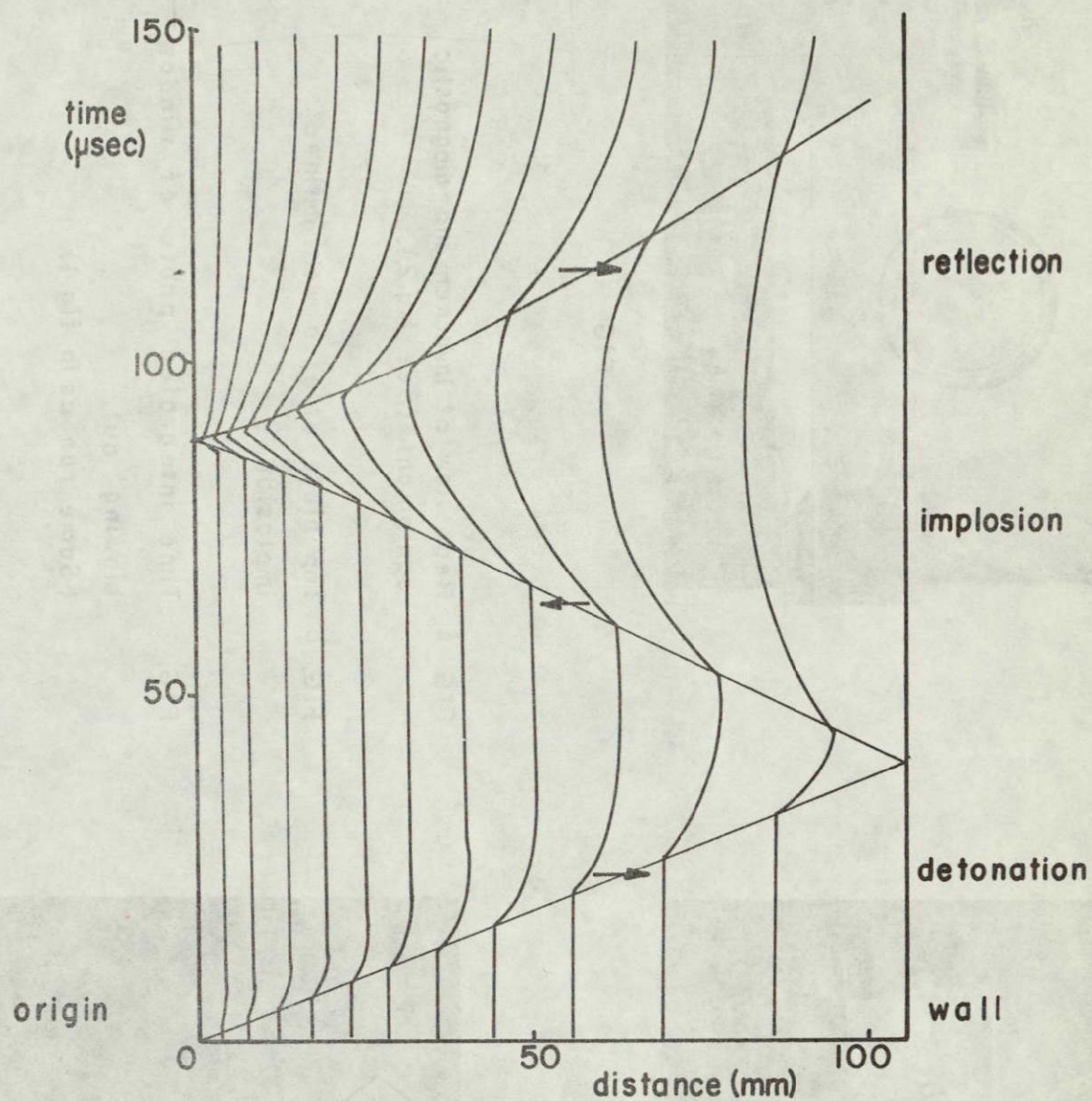
FIG. 43 X-t DIAGRAM AND PARTICLE PATHS FOR A COMBUSTION DRIVEN
SPHERICAL IMPLOSION WAVE (200 psi $2H_2 + O_2$)
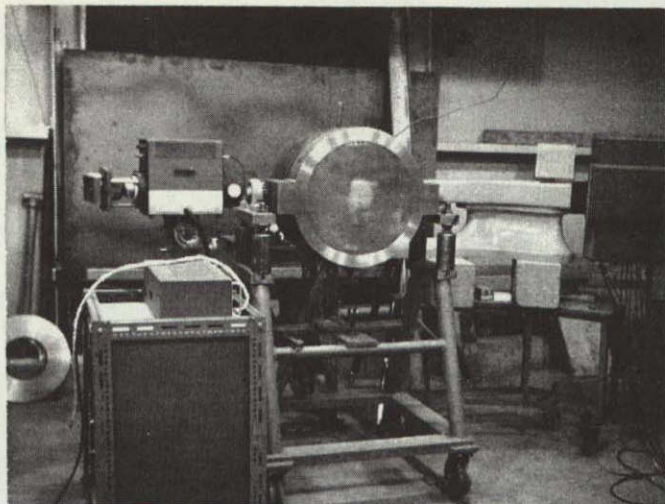
FIG. a
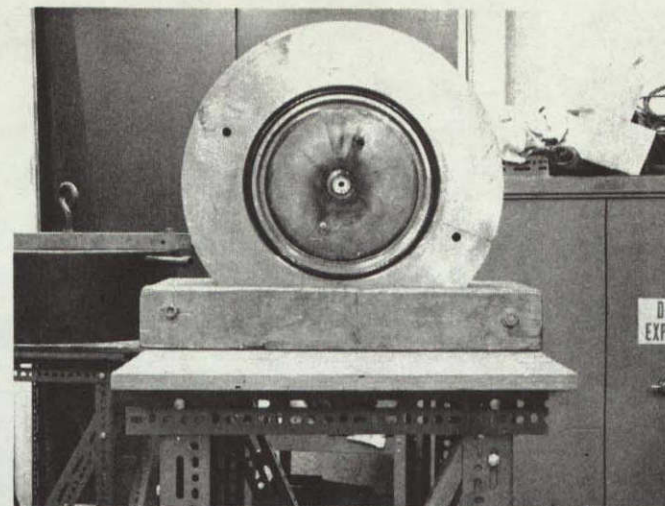
FIG. b

FIG. c

FIG. a. Rear view of launcher and diagnostic
equipment. (See fig. 2).

FIG. b Top plate after a well defined
implosion.

FIG. c Time integrated photo of window
blowing out.
(Same run as in fig. 4).

FIG. 44 PHYSICAL ARRANGEMENTS AND RESULTS

framing
camera

fully silvered
half silvered

expendable mirrors

spectrograph

quartz lens

photographic or photoelectric
recording device

live
electrode

gas
inlet

lock nut

copper plug

top plate

launcher cavity

expendable quartz window

exploding wire
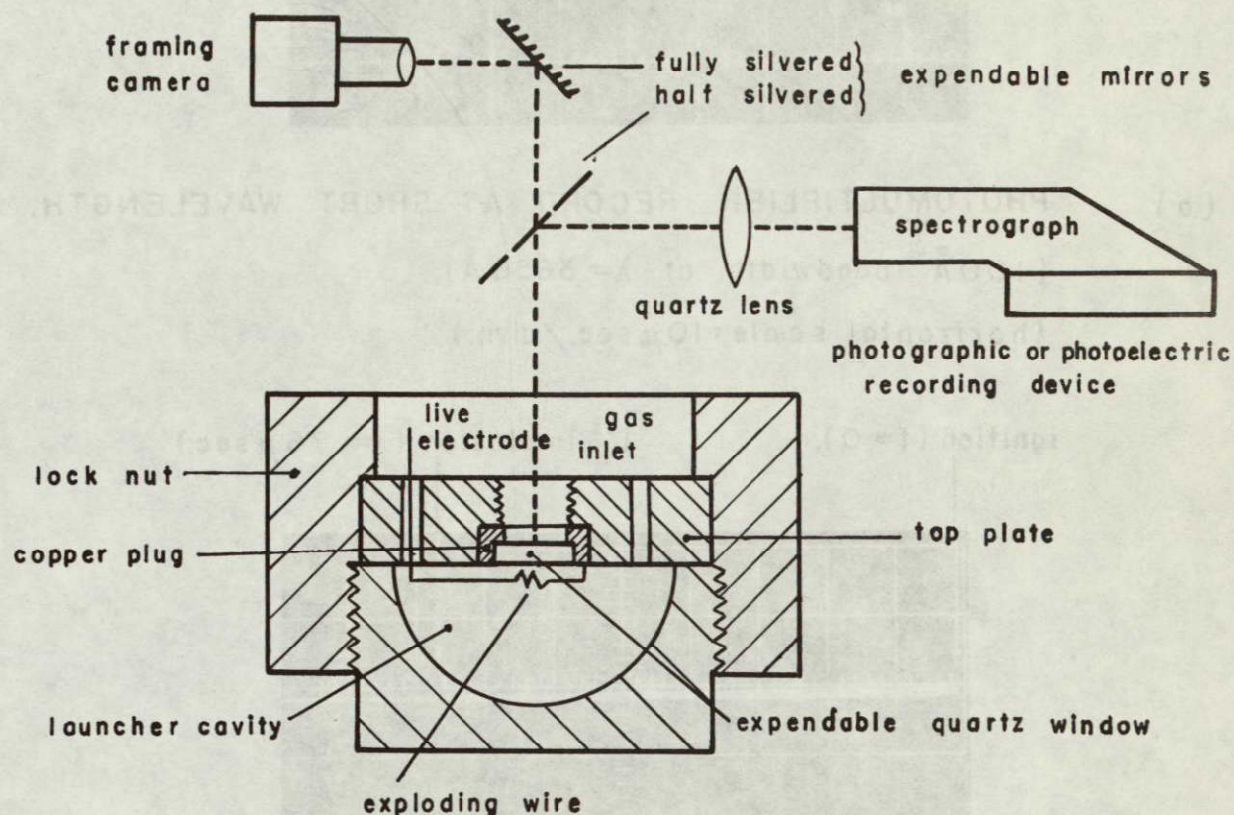
(a) GENERAL ARRANGEMENT (PLANVIEW).

exploding wire

7·5 μFd
6 K.V.

thyratron
switch

oscilloscopes

framing
camera

0—100
μsec.

variable
delay

manual
trigger

1 2   3 4   5 6
photomultiplier   signals
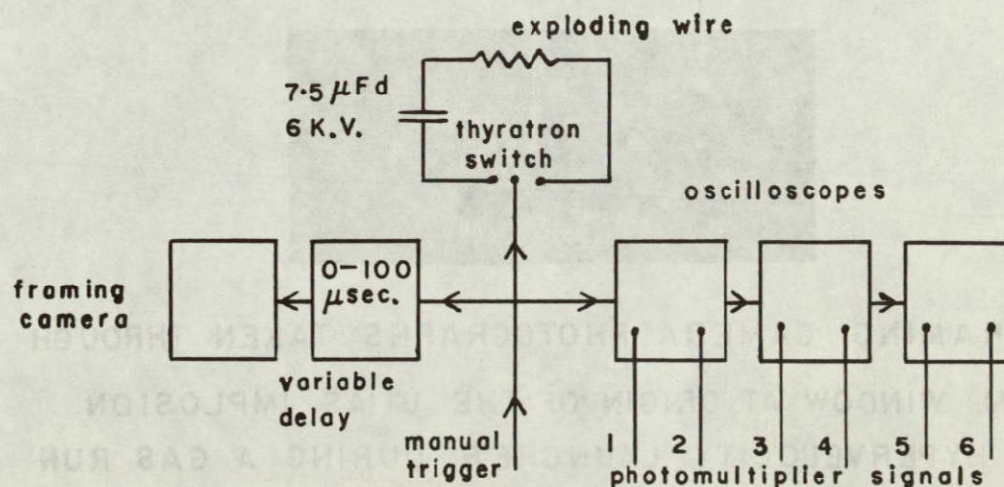
(b) SWITCHING PROCEDURE

FIG. 45 DIAGNOSTIC ARRANGEMENT.

45
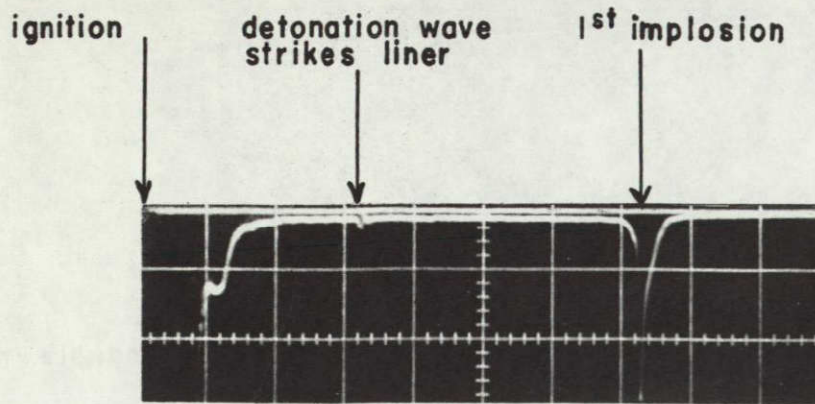
(a) PHOTOMULTIPLIER RECORD AT SHORT WAVELENGTH.

(100Å bandwidth at λ= 3656Å).

(horizontal scale: 10 μsec./divn.)
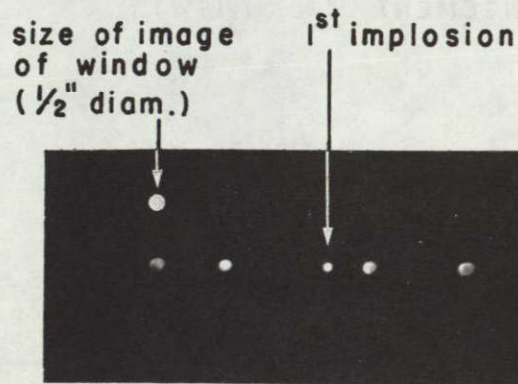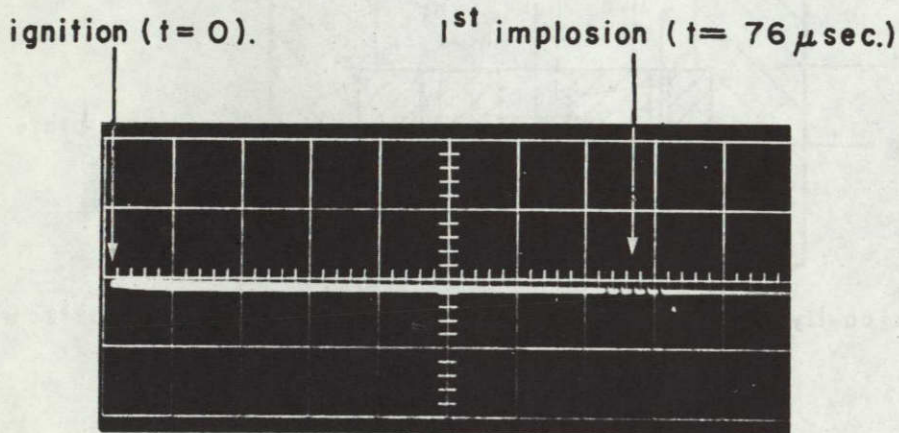
(b)

FIG 46 FRAMING CAMERA PHOTOGRAPHS TAKEN THROUGH

½ DIAM. WINDOW AT ORIGIN OF THE UTIAS IMPLOSION

DRIVEN HYPERVELOCITY LAUNCHER DURING A GAS RUN

(200 p.s.i. $2H_2 + O_2$).

(a) Timing markers (10 μ sec./divn.)

(b) Five frames at 2μsec. intervals (exposure times 0.1μsec.)
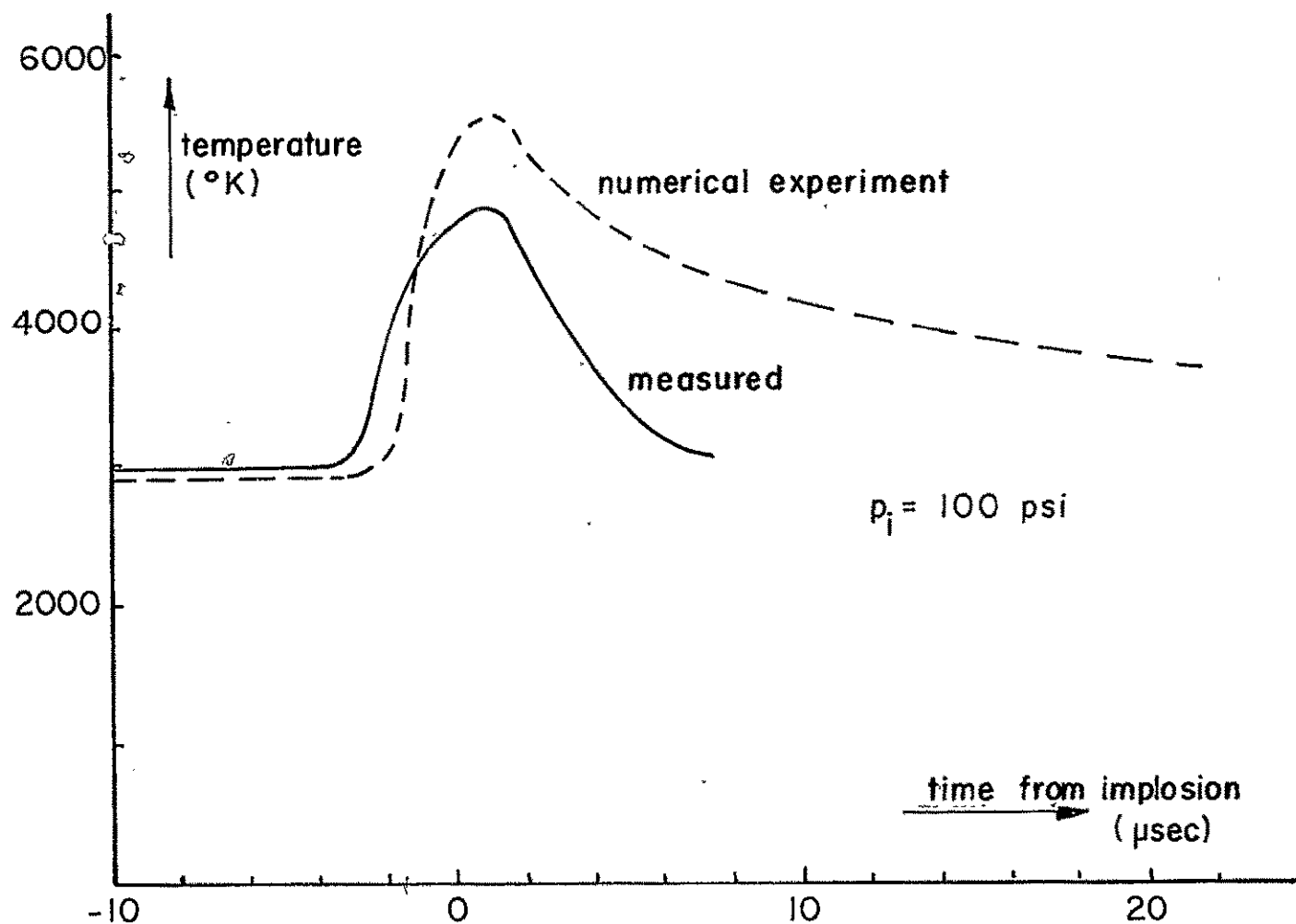
FIG. 47   COMPARISON BETWEEN MEASURED   AND COMPUTED
          AVERAGE TEMPERATURES AT THE ORIGIN
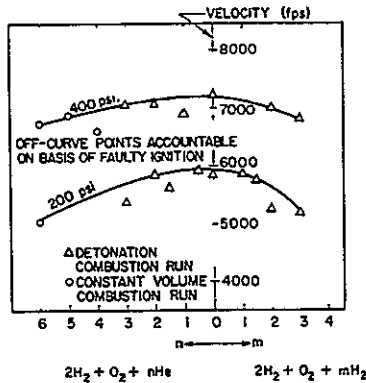
Figure 48
Muzzle velocities for diluted mixtures
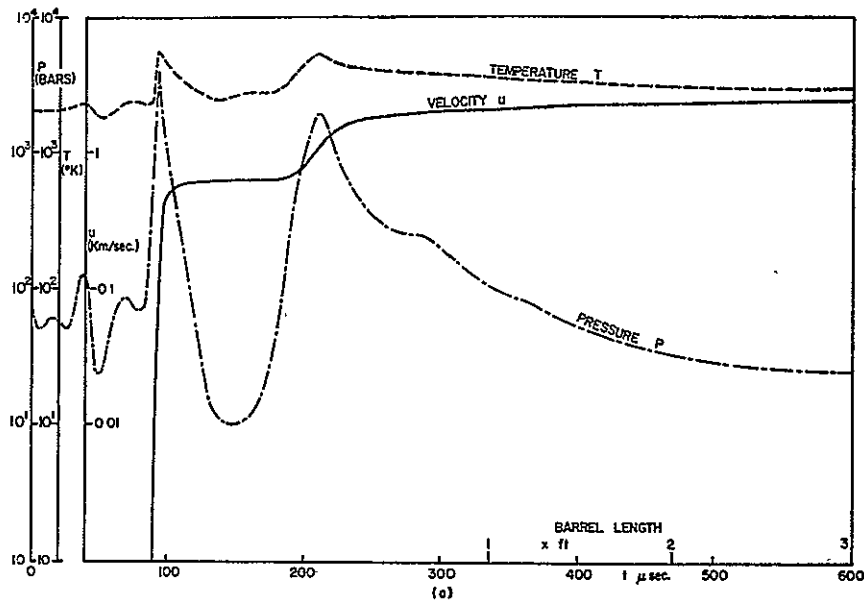
(a) Pressure and temperature at the base of the projectile and projectile velocity as a function of time and barrel length

Figure 49
Ideal performance of UTIAS implosion-driven hypervelocity launcher using a 200 psi, $2H_2 + O_2$ detonating driver gas. Chamber radius: 10.16 cm (4 in.); projectile: 0.55 cm (0.22 in.) dia. × 0.55 cm long polyethylene (0.92 gm/cm³) weighing 126 mg; gas energy: 44.8 K cal, $E_{proj}/E_{gas} = 0.0025$; acceleration in g's = 2×10^5 pressure in bars; at 6 ft. the muzzle velocity = 2.7 km/sec.
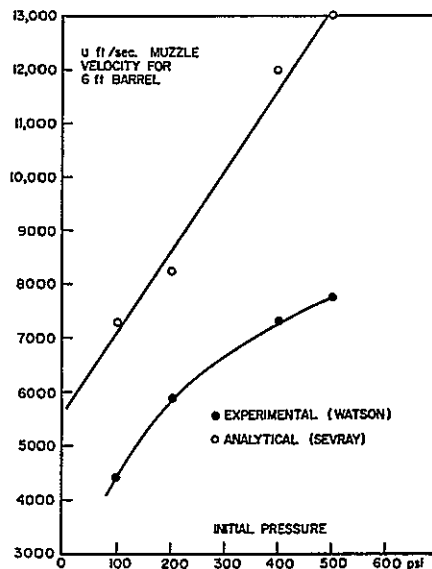
(b) Comparison of Sevray's analytical results with Watson's measured muzzle velocities for $2H_2 + O_2$ detonation runs in the initial pressure range $100 \leqslant p_i \leqslant 500$ psi

48
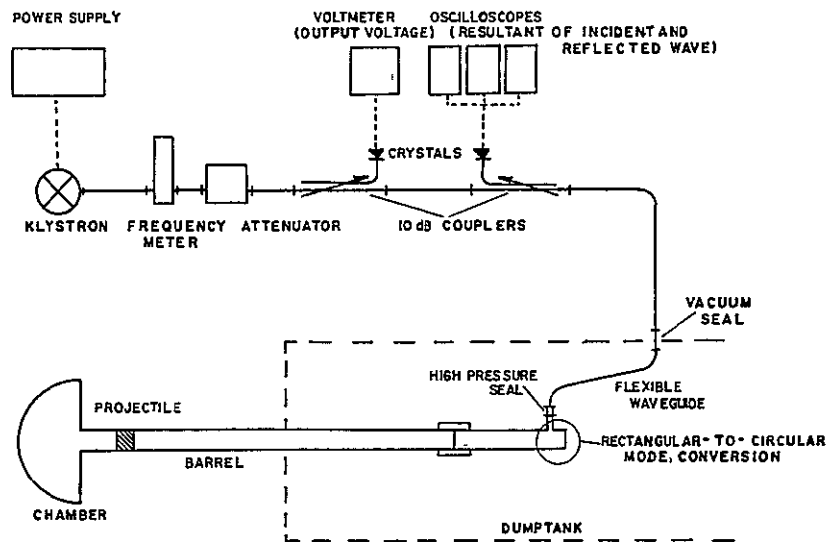
Figure 50   EXPERIMENTAL MICROWAVE SYSTEM

400 psi $2H_2 + O_2$

△ RUN 286 0 67 g proj. mass
× RUN 287 0.67 g proj. mass

5/16 in. dia. barrel
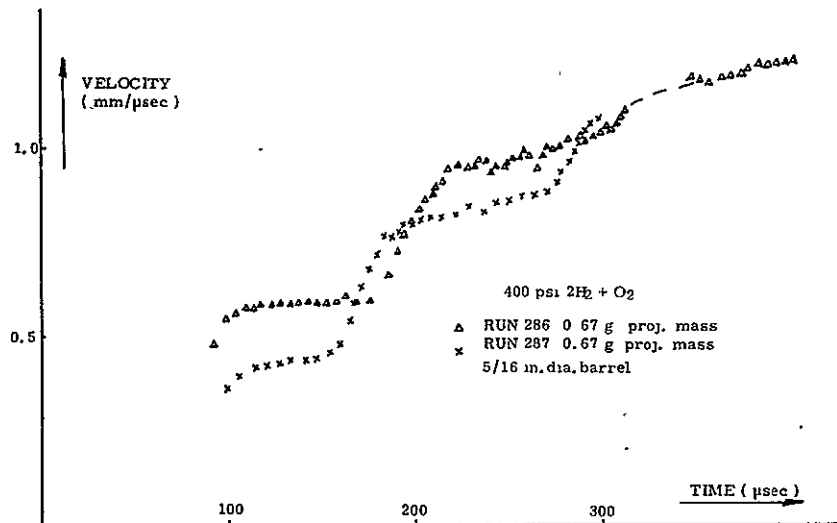
Figure 51   VELOCITY PROFILE 400 psi

EXPERIMENTAL RUN 286

COMPUTED

EXPERIMENTAL RUN 287

400 psi $2H_2 + O_2$
proj. mass 0.67 g
barrel   5/16" dia.
chamber   8 1/4 " dia.
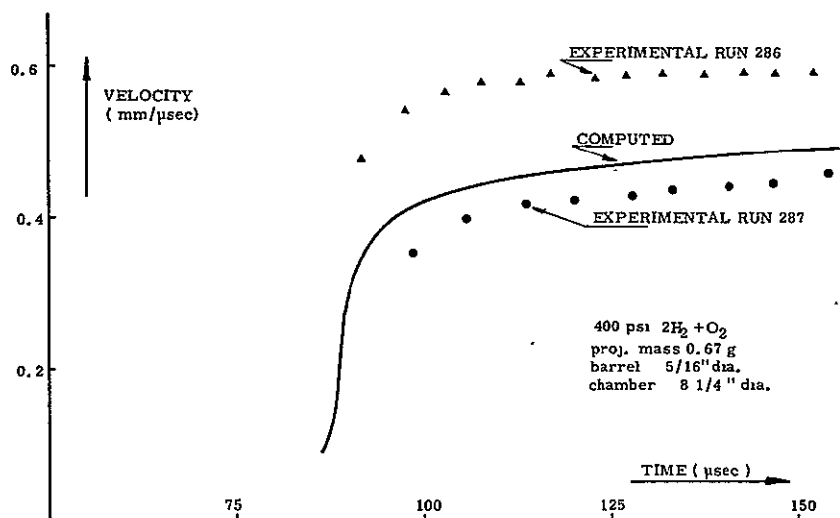
Figure 52   COMPARISON BETWEEN COMPUTED (REF. 6) AND MEASURED
INITIAL VELOCITIES
(400 psi)
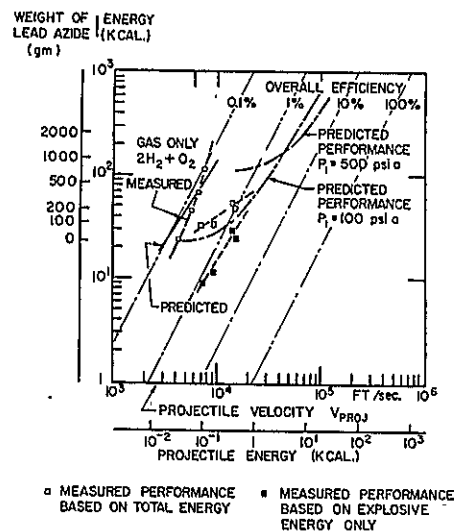
Figure 53
Measured and predicted performance using lead azide and
0.22 in. dia. 1 calibre polyethylene projectiles in a 60.0 in.
barrel and a stoichiometric oxygen-hydrogen mixture
at 100 psia

□ MEASURED PERFORMANCE   ■ MEASURED PERFORMANCE
BASED ON TOTAL ENERGY   BASED ON EXPLOSIVE
                                ENERGY ONLY
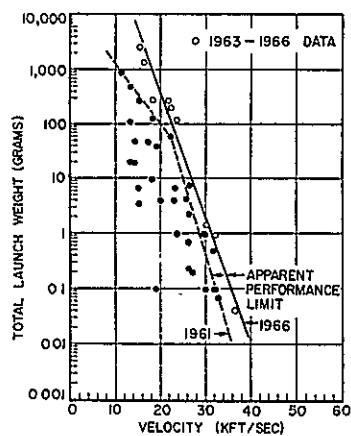
Figure 55
Maximum projectile launch velocities and weights—1966
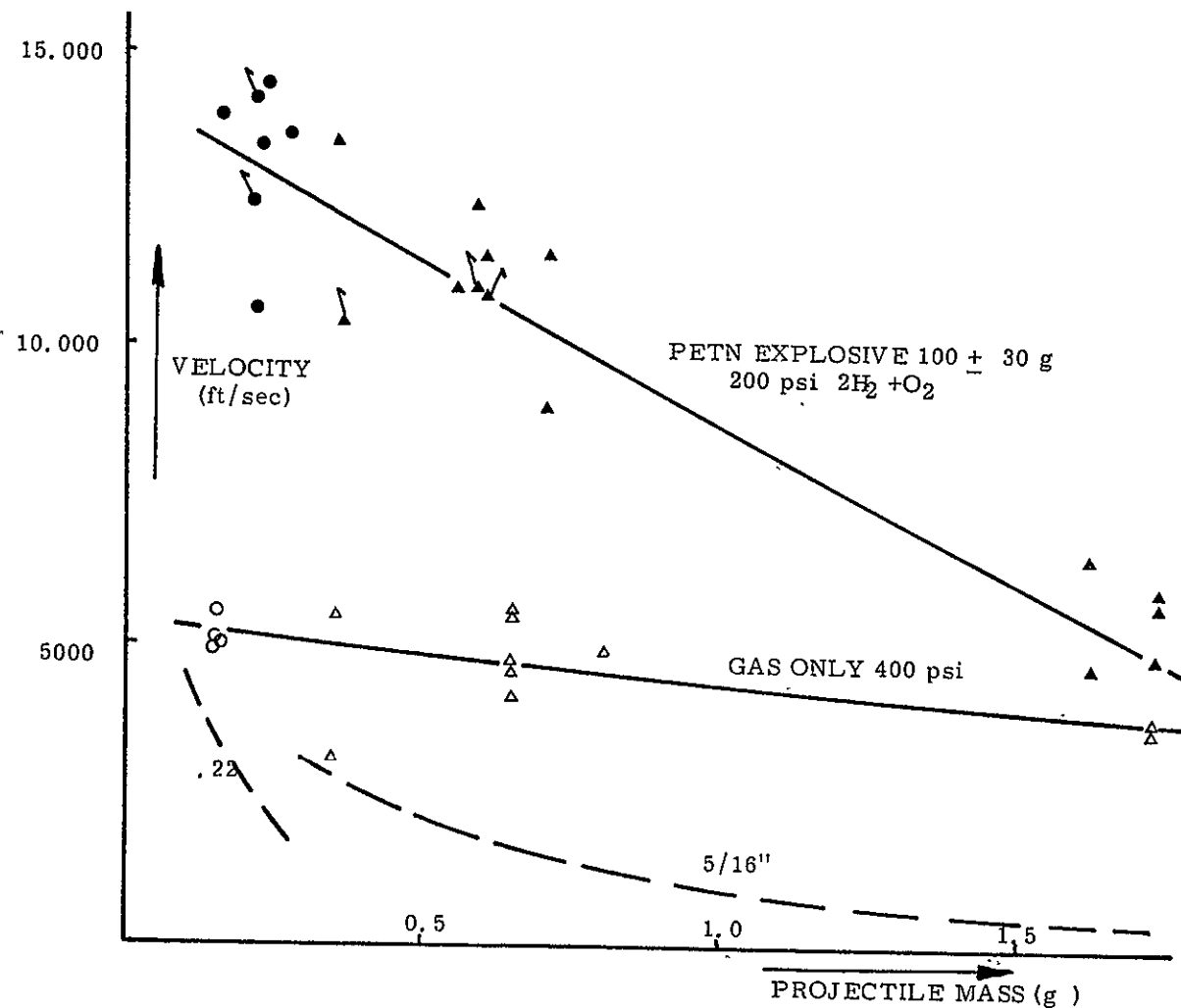
Figure 54   SAMPLE OF VELOCITY MEASUREMENTS, GAS AND EXPLOSIVE

● ○   3/16" or . 22 DIA. BARREL

▲ △   5/16 DIA. BARREL   BARREL LENGTH   5- 10 ft

↱   INDICATES PROJECTILE FAILURE

— — —   SCALED VELOCITY AFTER FIRST IMPLOSION
        (GAS CASE)

CONICAL LINER PLATE

2H₂+O₂

$2H_2 + O_2$

PROJECTILE

d_b

R_c

BARREL

PETN LINER

α

L_r

θ

a) **HEMISPHERICAL CAVITY**

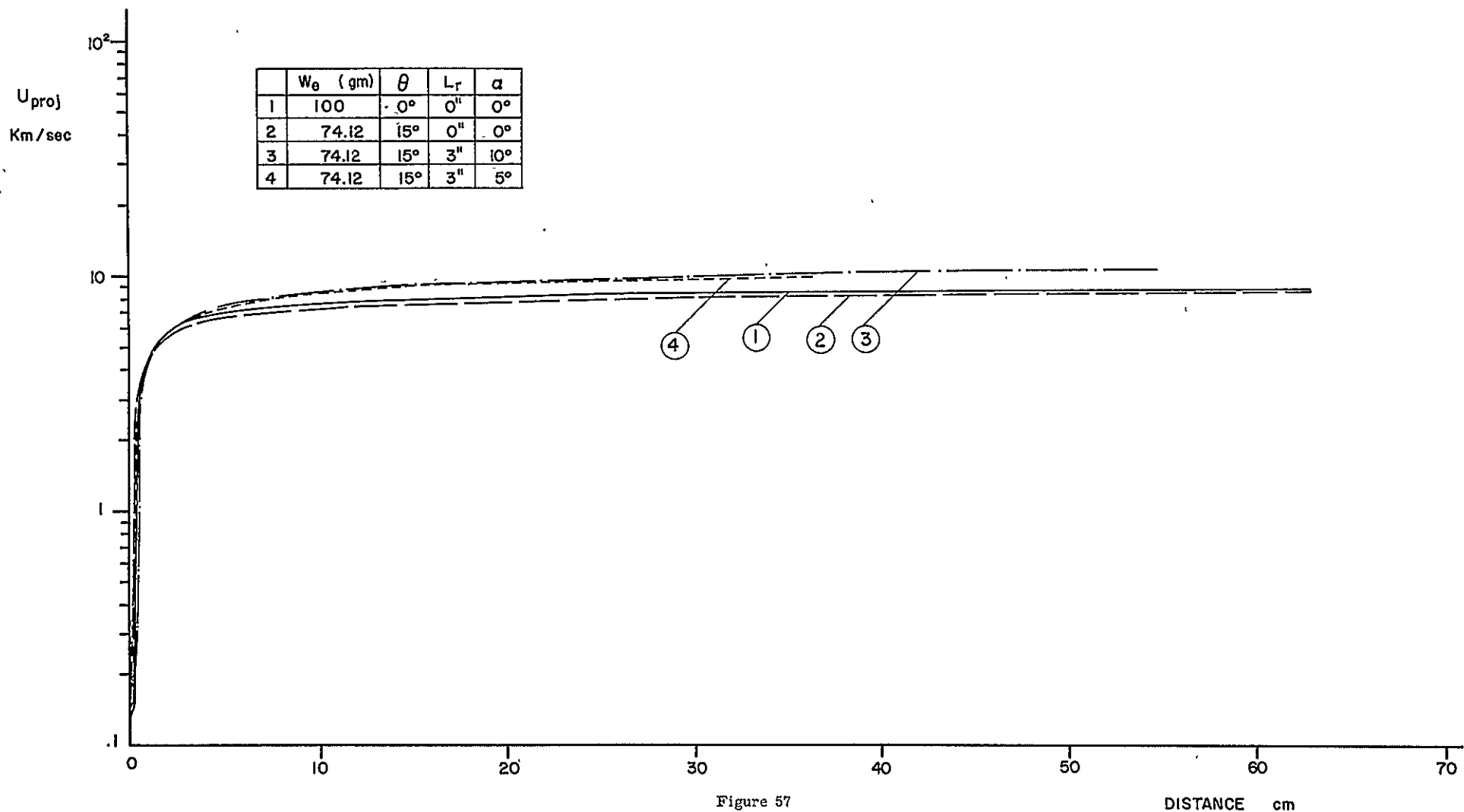b) **HEMISPHERICAL CAVITY WITH THE ADDITION OF A CONICAL LINER PLATE**
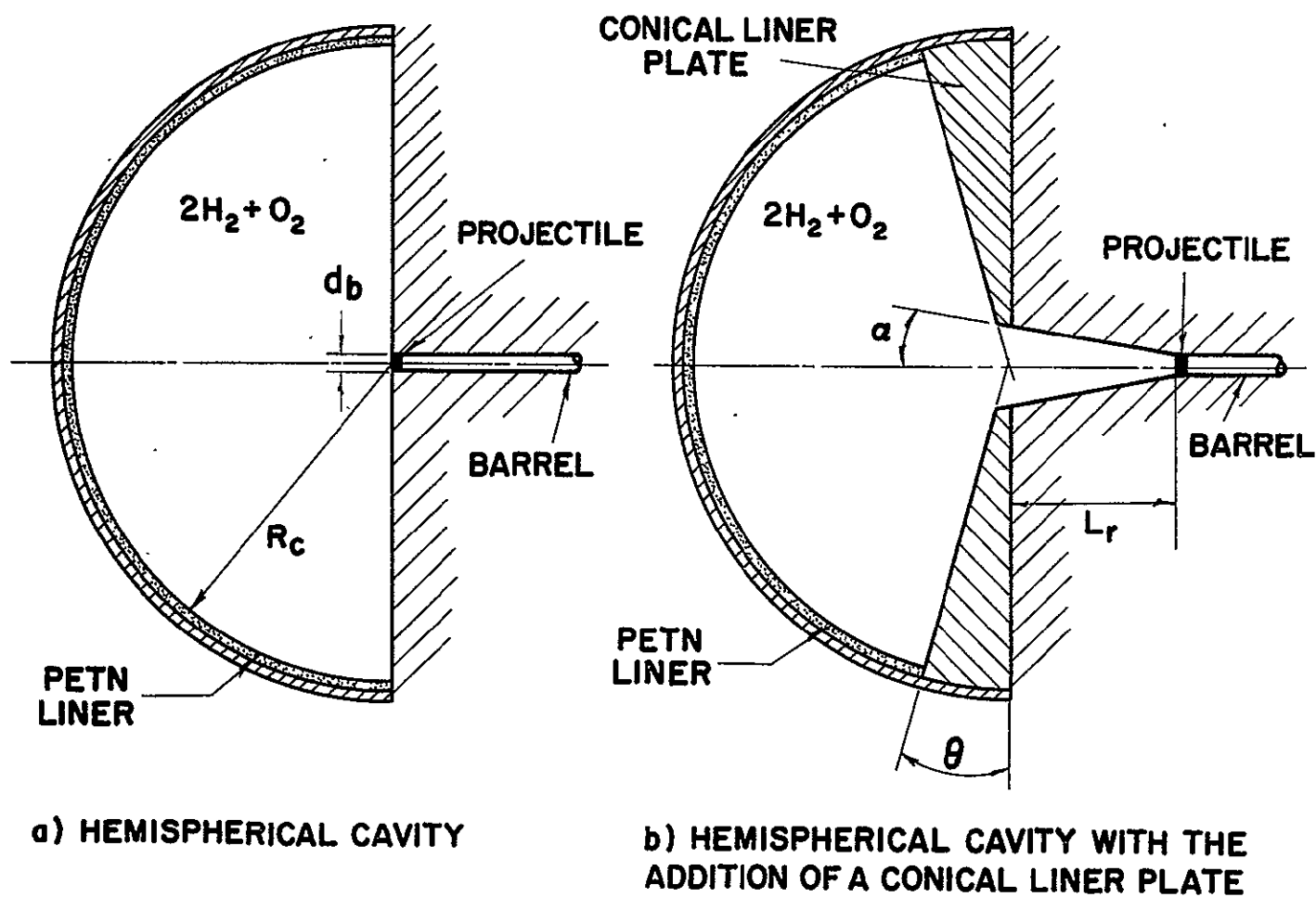
Figure 56

IMPLOSION CHAMBER GEOMETRIES USED IN THE COMPUTER CODES

The actual geometries were not very different except that smooth flared
entrances to the barrel were provided in both cases.

	W_θ (gm)	θ	L_r	α
1	100	0°	0"	0°
2	74.12	15°	0"	0°
3	74.12	15°	3"	10°
4	74.12	15°	3"	5°

U_{proj} Km / sec

DISTANCE cm

Figure 57

NUMERICAL SOLUTION OF PROJECTILE VELOCITY VS DISTANCE ALONG THE BARREL
OF A TYPICAL EXPERIMENTAL RUN

Driver gas $2H_2 + O_2$, 400 psi initial; half-calibre (0.22 in dia) titanium projectile, 0.29 g,
and a 7 7/8 in dia chamber. Various weights of explosives with and without a conical
liner, recess, and flare angle are shown in the table. The amount of explosive and
geometrical factors have not been optimized for maximum muzzle velocity.
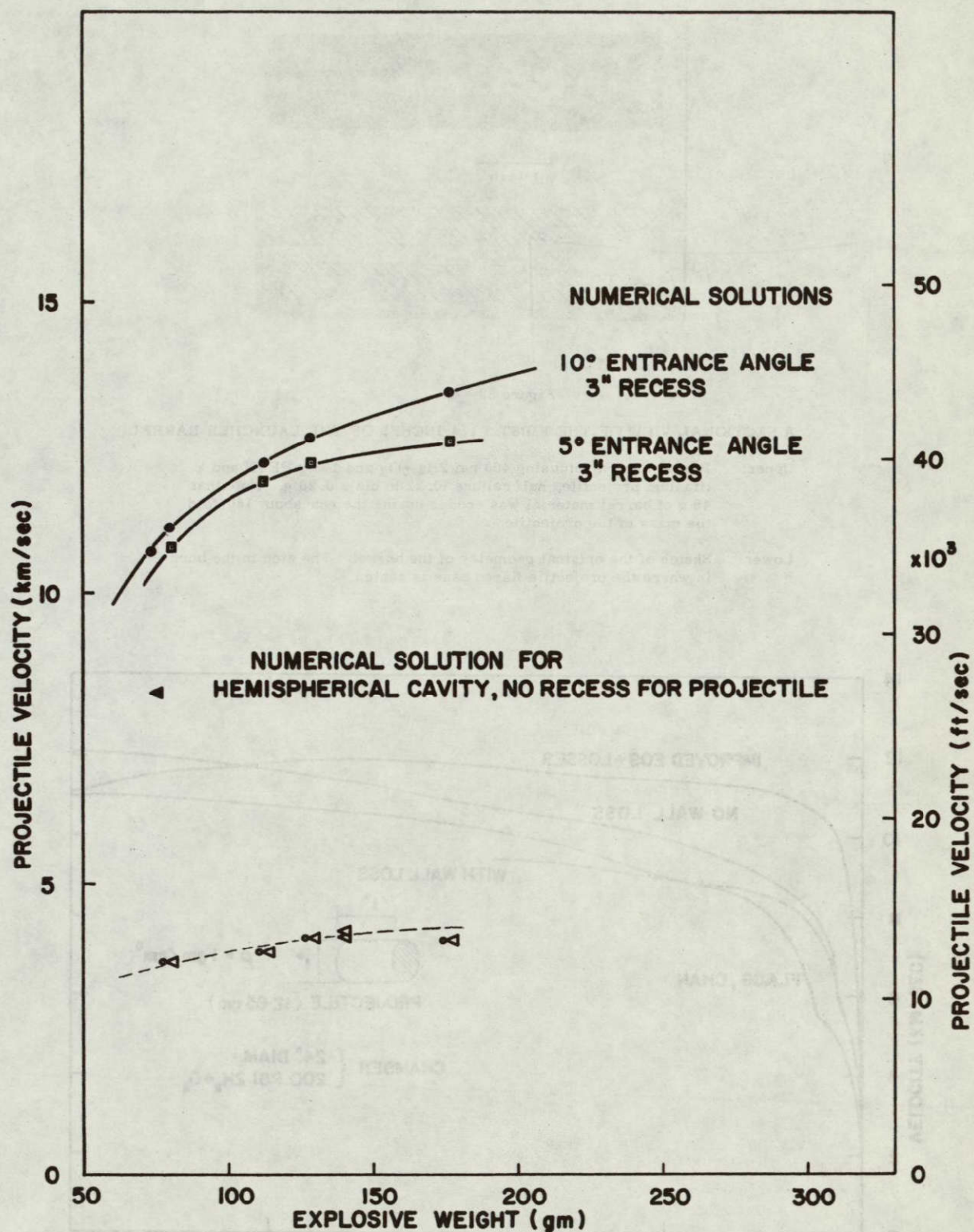
Figure 58

COMPARISON OF NUMERICAL AND EXPERIMENTAL PERFORMANCE OF THE MARK III
LAUNCHER OF PROJECTILE VELOCITY VS PETN WEIGHT

Driver gas $2H_2 + O_2$, 400 psi initial; half-calibre (0.22 in dia) titanium projectile, 0.29 g;
upper discrete points are numerical results, lower discrete points are for focused implosions
(open triangle) and off-focus runs (attached circle). The amount of explosive is by no means
an optimum nor that of the recess or entrance angle for the 15-degree protector plate-
optimum calculated values yield about 50,000 ft/sec.

53
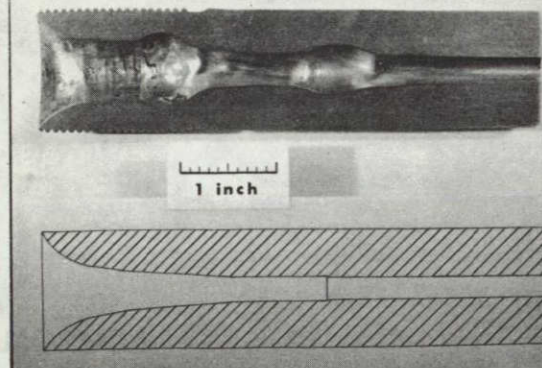
Figure 59

A SECTIONAL VIEW OF THE FIRST 5 1/4-INCHES OF THE LAUNCHER BARREL

Upper: Barrel after a run using 400 psi $2H_2 + O_2$ and 143 g PETN and a
          titanium projectile, half calibre (0.22 in dia), 0.28 g. Note that
          45 g of barrel material was eroded during the run-about 160-fold
          the mass of the projectile.

Lower: Sketch of the original geometry of the barrel. The step in the bore
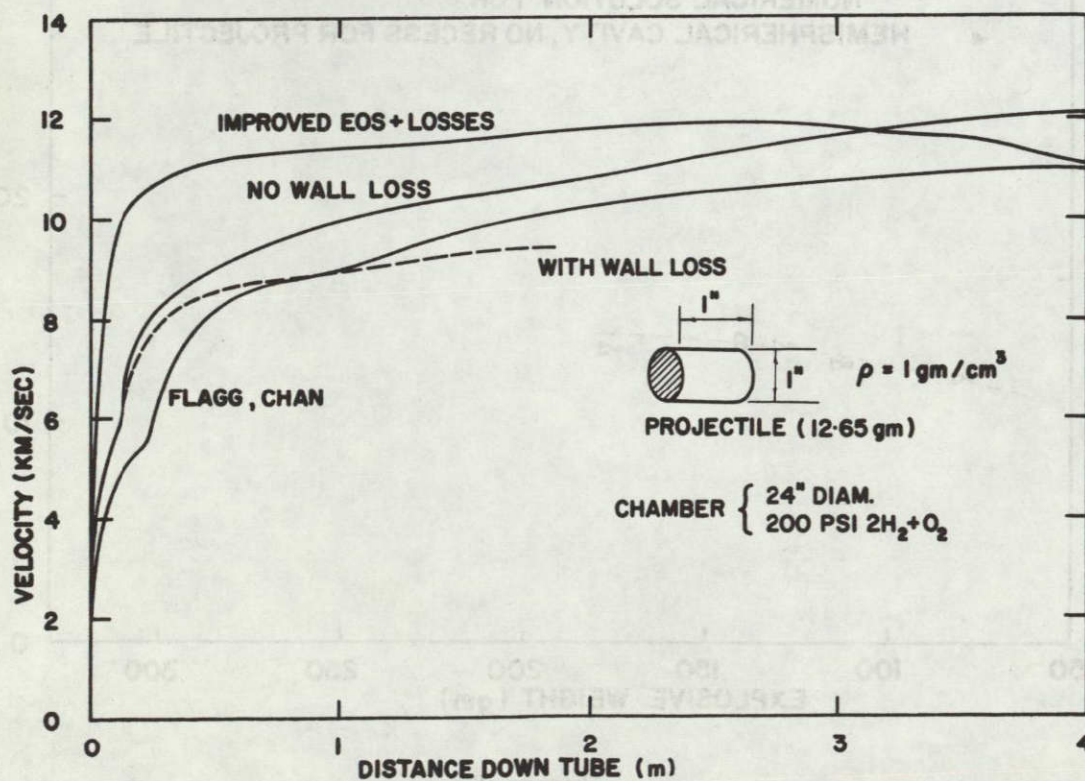   is where the projectile flared base is seated.

Figure 60

PROJECTILE VELOCITY VS LAUNCHER BARREL LENGTH FROM SEVERAL SOLUTIONS
BY BRODE (REF. 35) AND FLAGG-CHAN (REF. 15)

Brode's no wall loss may be compared with Flagg-Chan showing very good agreement
between the two independent analyses. Brode's improved equation of state (EOS)+losses
shows a suprising improvement in performance, despite losses, resulting from increased
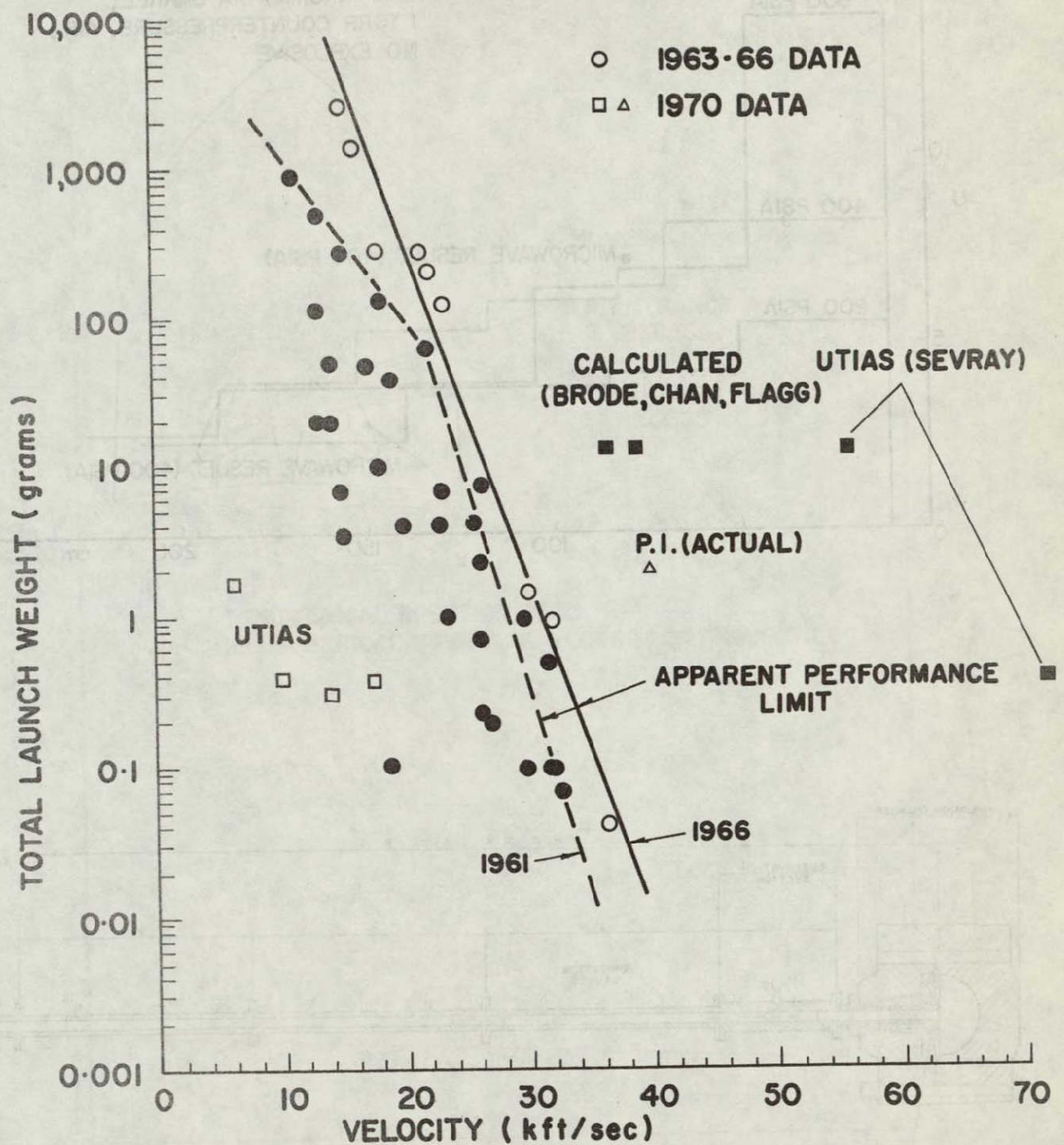pressure and density from the eroded barrel constituents.

Figure 61

ACTUAL AND CALCULATED PROJECTILE MUZZLE VELOCITY
VS PROJECTILE WEIGHT (AFTER REFS. 43, 44) WITH ADDED
RESULTS FROM UTIAS(REFS. 2, 15) AND PHYSICS INTERNATIONAL
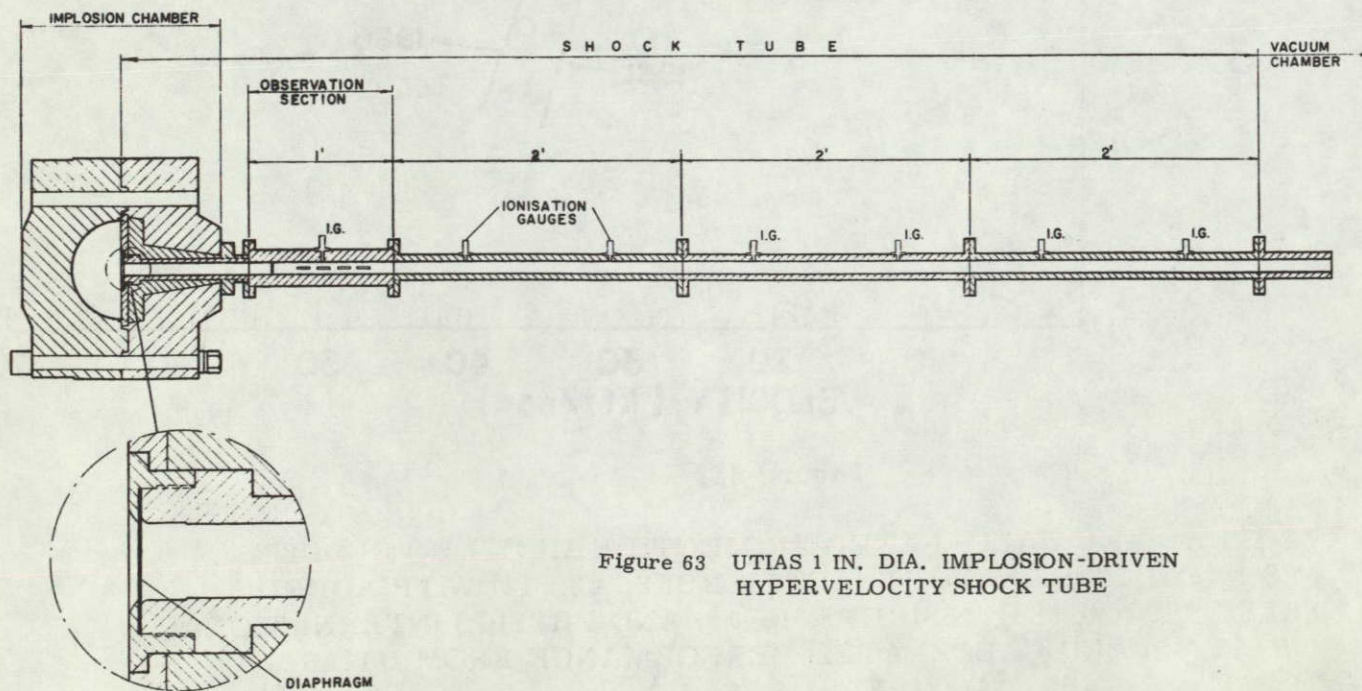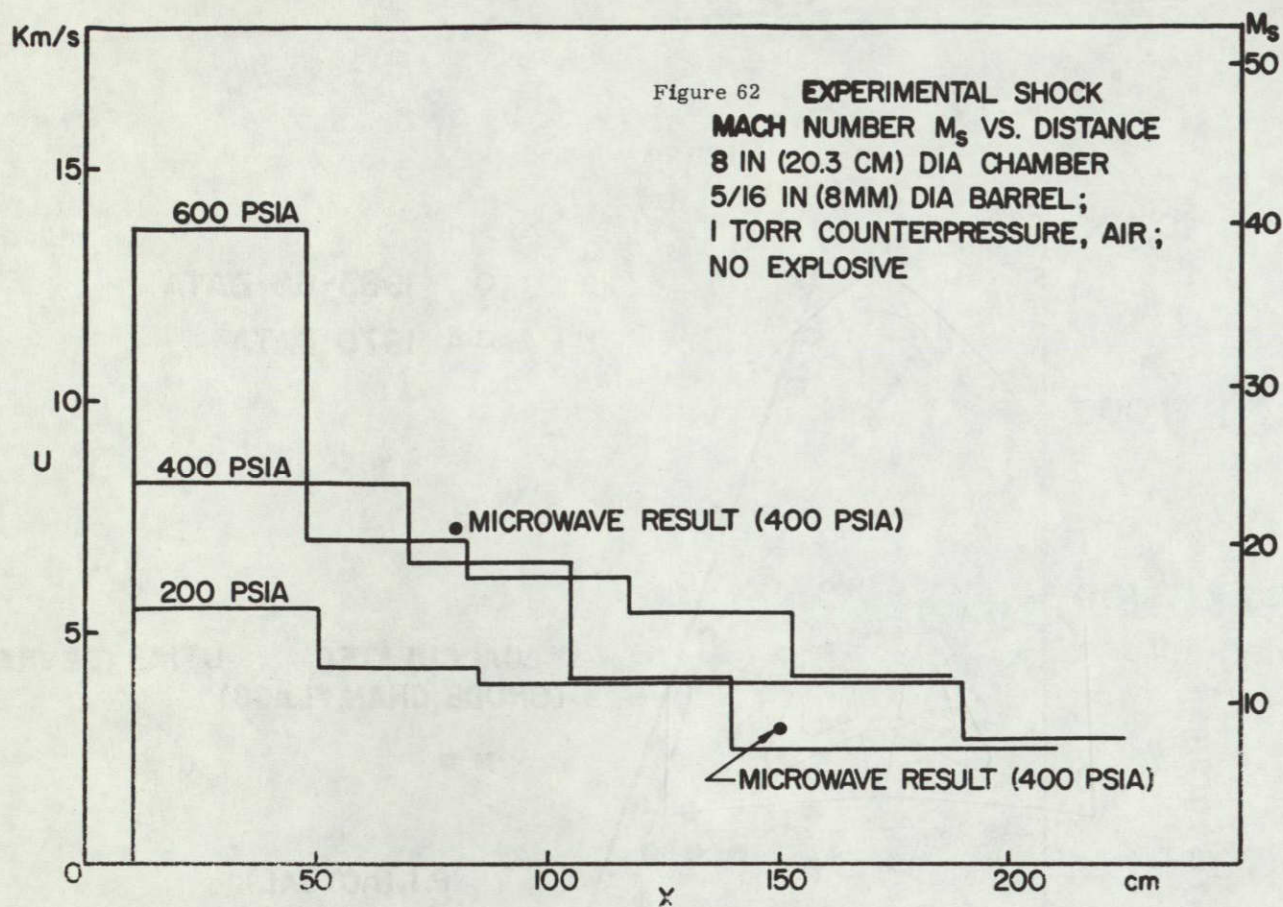(REF. 45) AND CALCULATED PERFORMANCE FROM UTIAS
(REFS. 5, 6, 15)

Figure 62   EXPERIMENTAL SHOCK MACH NUMBER M_s VS. DISTANCE 8 IN (20.3 CM) DIA CHAMBER 5/16 IN (8MM) DIA BARREL; I TORR COUNTERPRESSURE, AIR; NO EXPLOSIVE

Figure 63   UTIAS 1 IN. DIA. IMPLOSION-DRIVEN HYPERVELOCITY SHOCK TUBE
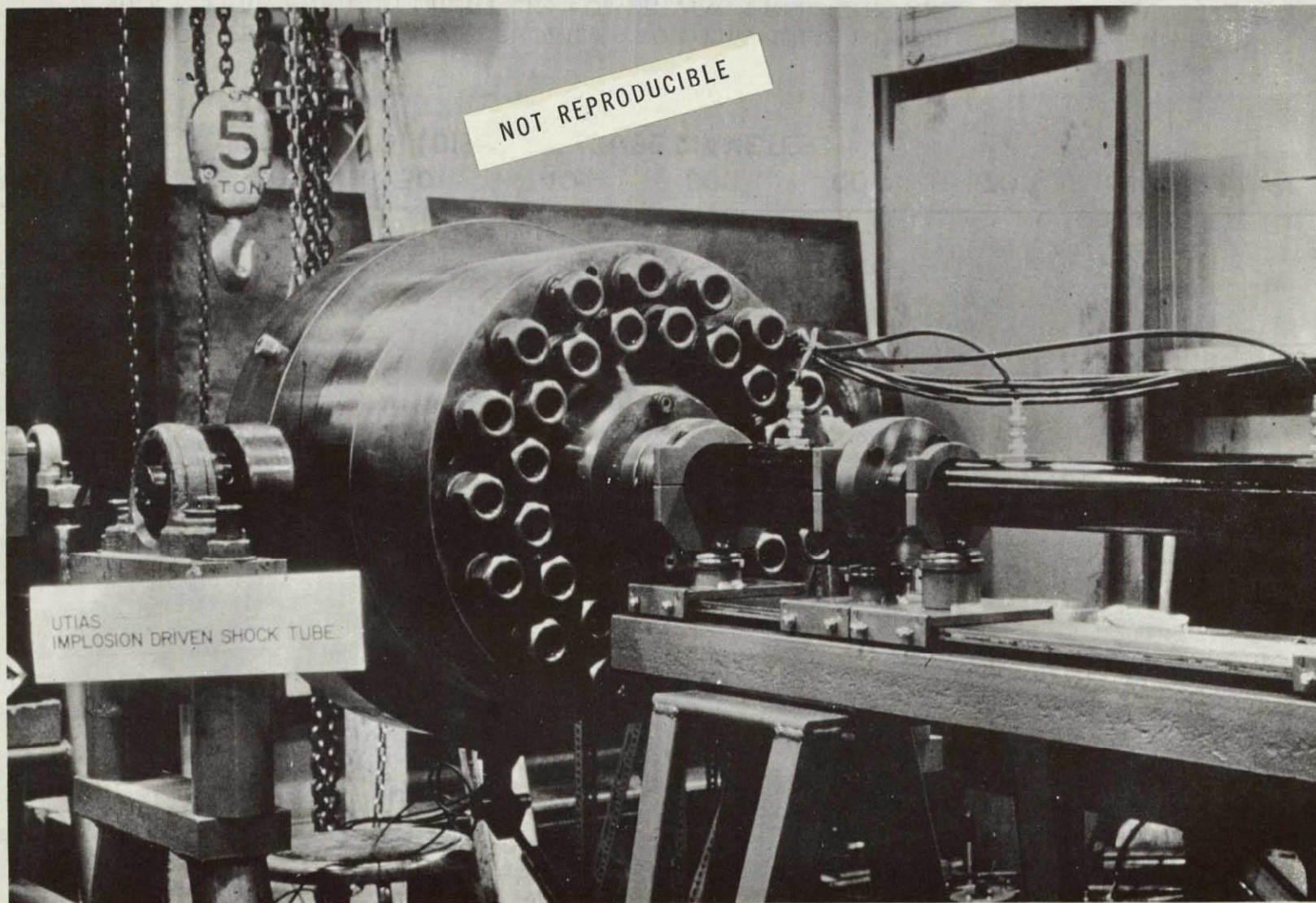
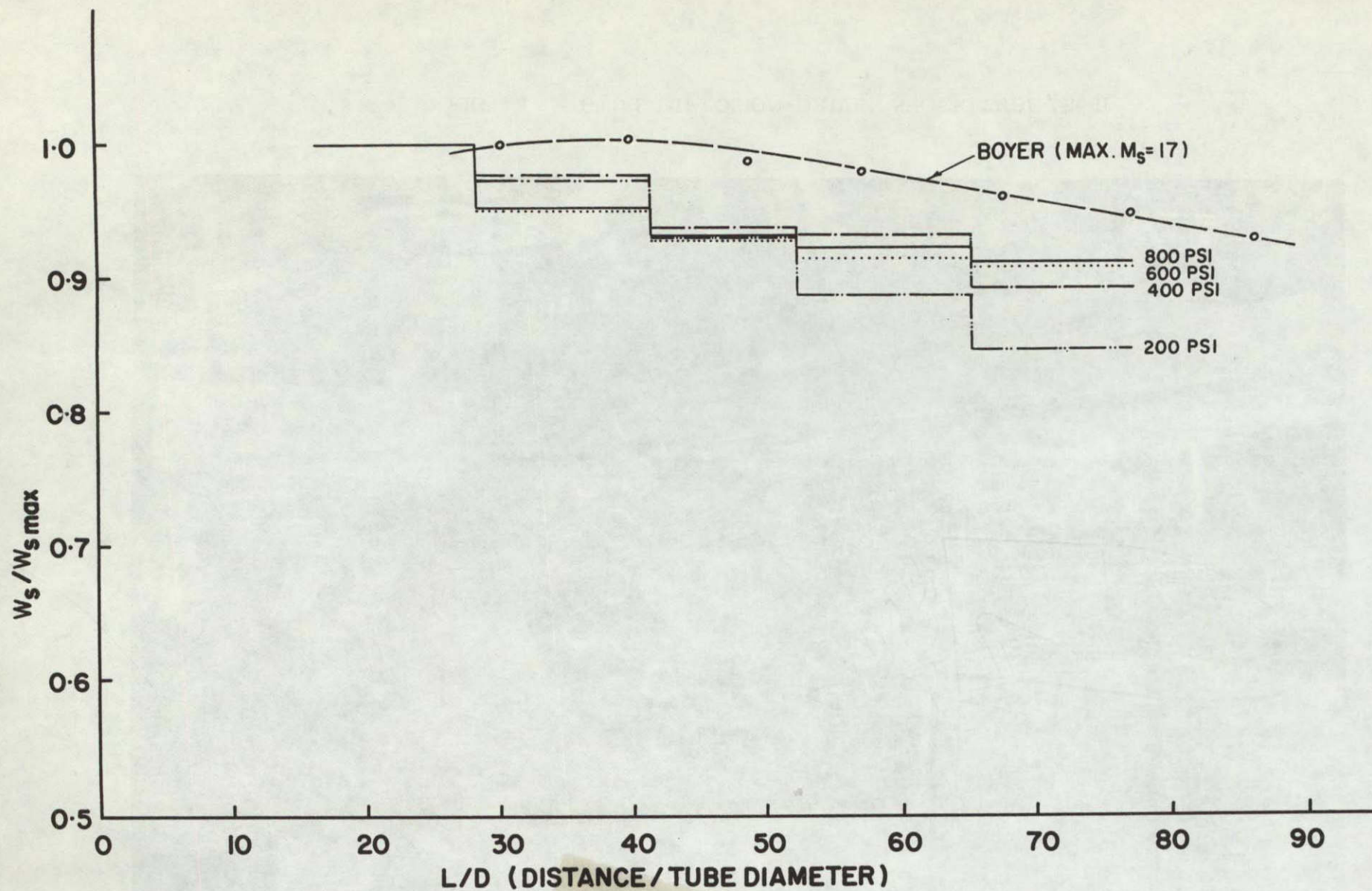2

FIG 64   UTIAS IMPLOSION-DRIVEN SHOCK TUBE MK II

Figure 65

NORMALIZED ATTENUATION PROFILES FOR THE UTIAS 1 IN DIA IMPLOSION-DRIVEN
SHOCK TUBE FOR DIFFERENT $2H_2 + O_2$ DRIVING PRESSURES AND A CHANNEL PRESSURE
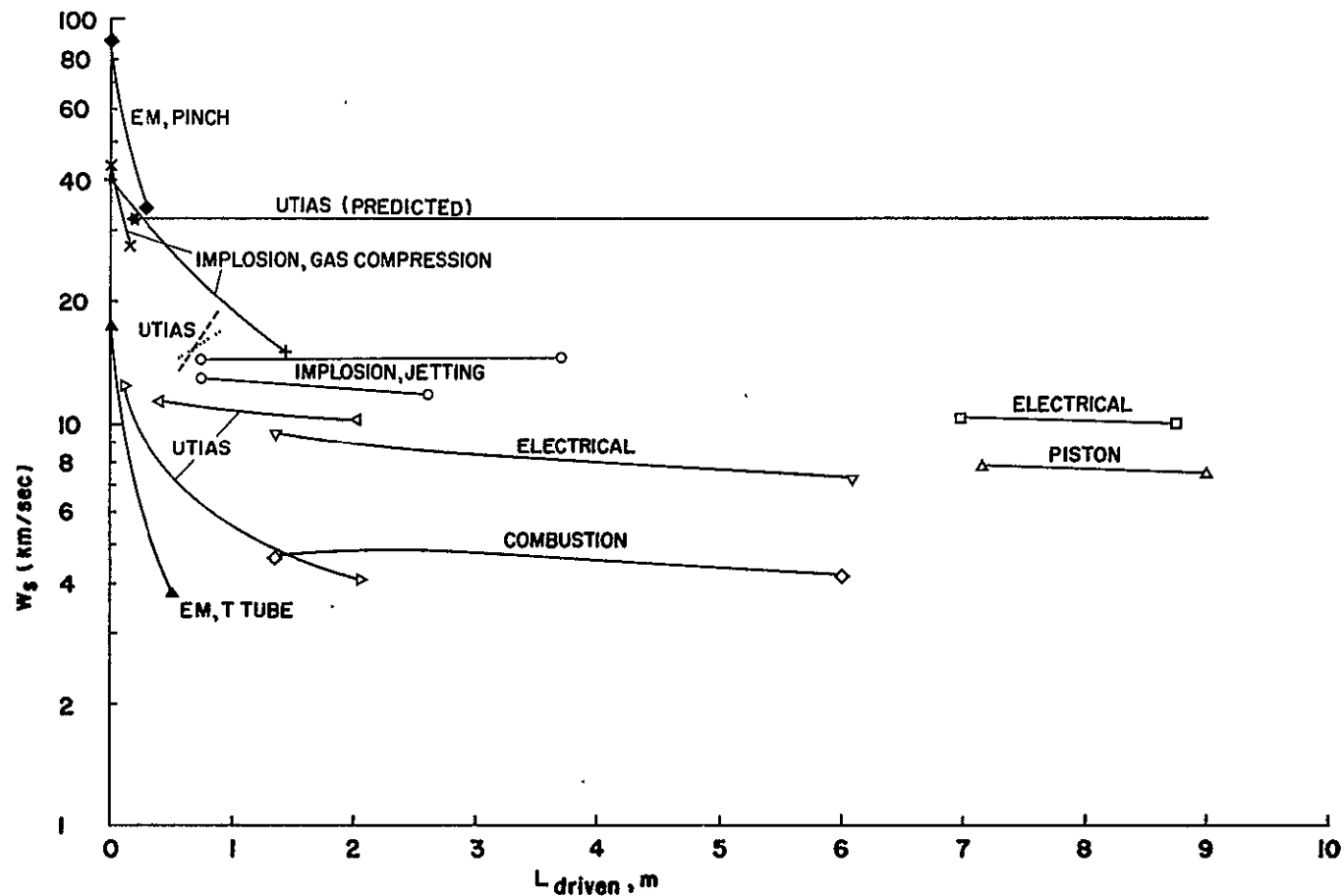OF 1 MM HG AIR

Figure 66

SHOCK TUBE PERFORMANCE USING A VARIETY OF DRIVING TECHNIQUES
(after Ref. 48)

UTIAS results: for air, p_1 = 1. 0 torr
----- 1"dia tube, $2H_2 + O_2$(400 psi) + 96 g PETN, experimental
..... 1"dia tube, $2H_2 + O_2$(400 psi) + 84 g PETN, experimental
*   5/16"dia tube, $2H_2 + O_2$ (200 psi) + 200 g PETN, predicted
◁   1" dia tube, $2H_2 + O_2$ (800 psi) experimental
▷   5/16"dia tube, $2H_2 + O_2$ (600 psi) experimental
Other results:

+	Crowley & Glenn, 1969, p_1 = 1 atm;	x	Voitenko, 1966, p_1 = 1 atm
o	Gill & Goettelman, 1967, 5 torr	◻	Gruszczynski & Rogers, 1964, 0. 5 torr
▲	Willard, 1967, 0. 05 torr	▼	Hoppman & Glick, 1967, 0. 5 torr
◊	Rose & Nelson, 1958, 10 torr	▲	Dukowicz, 1963, 3 torr
◆	Josephson & Hales, 0. 5 torr		

NASA
FORMAL
REPORT